

REPORT DOCUMENTATION PAGE			Form Approved OMB NO. 0704-0188		
<p>The public reporting burden for this collection of information is estimated to average 1 hour per response, including the time for reviewing instructions, searching existing data sources, gathering and maintaining the data needed, and completing and reviewing the collection of information. Send comments regarding this burden estimate or any other aspect of this collection of information, including suggestions for reducing this burden, to Washington Headquarters Services, Directorate for Information Operations and Reports, 1215 Jefferson Davis Highway, Suite 1204, Arlington VA, 22202-4302. Respondents should be aware that notwithstanding any other provision of law, no person shall be subject to any penalty for failing to comply with a collection of information if it does not display a currently valid OMB control number. PLEASE DO NOT RETURN YOUR FORM TO THE ABOVE ADDRESS.</p>					
1. REPORT DATE (DD-MM-YYYY) 30-08-2019		2. REPORT TYPE Final Report		3. DATES COVERED (From - To) 14-Apr-2016 - 13-Apr-2019	
4. TITLE AND SUBTITLE Final Report: Uncovering the cause of ratcheting and low-cycle fatigue [1.2 Solid Mechanics]			5a. CONTRACT NUMBER W911NF-16-1-0159		
			5b. GRANT NUMBER		
			5c. PROGRAM ELEMENT NUMBER 611102		
6. AUTHORS			5d. PROJECT NUMBER		
			5e. TASK NUMBER		
			5f. WORK UNIT NUMBER		
7. PERFORMING ORGANIZATION NAMES AND ADDRESSES University of Florida - Gainesville 219 Grinter Hall PO Box 115500 Gainesville, FL 32611 -5500			8. PERFORMING ORGANIZATION REPORT NUMBER		
9. SPONSORING/MONITORING AGENCY NAME(S) AND ADDRESS (ES) U.S. Army Research Office P.O. Box 12211 Research Triangle Park, NC 27709-2211			10. SPONSOR/MONITOR'S ACRONYM(S) ARO		
			11. SPONSOR/MONITOR'S REPORT NUMBER(S) 68272-EG.10		
12. DISTRIBUTION AVAILABILITY STATEMENT Approved for public release; distribution is unlimited.					
13. SUPPLEMENTARY NOTES The views, opinions and/or findings contained in this report are those of the author(s) and should not be construed as an official Department of the Army position, policy or decision, unless so designated by other documentation.					
14. ABSTRACT					
15. SUBJECT TERMS					
16. SECURITY CLASSIFICATION OF:			17. LIMITATION OF ABSTRACT UU	15. NUMBER OF PAGES	19a. NAME OF RESPONSIBLE PERSON Oana Cazacu
a. REPORT UU	b. ABSTRACT UU	c. THIS PAGE UU			19b. TELEPHONE NUMBER 850-833-9350

RPPR Final Report

as of 16-Sep-2019

Agency Code:

Proposal Number: 68272EG

Agreement Number: W911NF-16-1-0159

INVESTIGATOR(S):

Name: Oana Cazacu
Email: cazacu@reef.ufl.edu
Phone Number: 8508339350241
Principal: Y

Organization: **University of Florida - Gainesville**

Address: 219 Grinter Hall, Gainesville, FL 326115500

Country: USA

DUNS Number: 969663814

EIN: 596002052

Report Date: 13-Jul-2019

Date Received: 30-Aug-2019

Final Report for Period Beginning 14-Apr-2016 and Ending 13-Apr-2019

Title: Uncovering the cause of ratcheting and low-cycle fatigue [1.2 Solid Mechanics]

Begin Performance Period: 14-Apr-2016

End Performance Period: 13-Apr-2019

Report Term: 0-Other

Submitted By: Oana Cazacu

Email: cazacu@reef.ufl.edu

Phone: (850) 833-9350241

Distribution Statement: 1-Approved for public release; distribution is unlimited.

STEM Degrees: 1

STEM Participants: 0

Major Goals: The overall goal of the proposed research is to advance the fundamental understanding of low cycle fatigue (LCF) under multiaxial loadings by proposing a novel modeling framework. Experimental data on metallic materials indicates that fracture due to ratcheting is preceded by some plastic deformation in the vicinity of the crack tip.

While significant progress has been made in development of experimental techniques for small-scale testing that enable improved accuracy in the measurement of the plastic zone for engineering structural materials, there are no models that can predict the manner in how the particularities of the plastic deformation affect crack growth.

Moreover, plasticity-damage couplings have not been addressed.

Major goals:

- develop a novel framework for modeling plasticity-damage couplings for isotropic materials;
- establish correlations between plastic properties and the rate of damage growth;
- develop elastic stress fields that do not violate the boundary conditions for elliptical crack problem;
- establish correlations between mechanical properties and the extent of plastic zone in front of a crack;
- develop potential accounting for plastic anisotropy to further assist in understanding the role of anisotropy on fatigue crack growth rate.

Accomplishments: Accomplishments related to analysis and prediction of the extent of the plastic zone in front of a crack tip:

-Developed new complex potentials and new solution to the biharmonic equation (Airy stress function)

-Based on the new Airy stress function obtained a new elastic solution for the stresses and strains in the vicinity of cracks

-This exact solution resolves the issues associated to the state-of-the-art approximate solution. Specifically, classic solution predicts stress state is axisymmetric ($\sigma_{xx} = \sigma_{yy}$) leading to inaccuracies in the estimate of near-crack tip behavior.

-According to the new analytical solution:

o σ_{xx} is no longer equal to σ_{yy}

o At the crack tip, σ_{yy} has an extremely large but finite value while $\sigma_{xx} = 0$ i.e. the boundary conditions are satisfied (the crack surface is traction free).

-Comparison with F. E. simulations shows the importance of fulfilling the remote boundary conditions and the boundary conditions at the crack boundary.

Accomplishments related to establishing correlations between plastic properties and the rate of damage growth:

-Established what are the plastic properties that affect the extent of the plastic zone near a crack

RPPR Final Report as of 16-Sep-2019

- Developed new analytical relations for rate of crack growth, which account for yielding characteristics
- Demonstrated that the upper bound for the size of the plastic zone is obtained for materials obeying Tresca yield condition (e.g. aluminum alloys).

Accomplishments related to development of new potentials:

- Developed new isotropic criterion that describes well yielding of randomly oriented face-centered polycrystalline metallic materials
- Developed the extension of this criterion such as to describe orthotropy was also developed using generalized invariants of the stress deviator. This new orthotropic criterion is general and applicable to three-dimensional stress states.
- Developed a novel potential expressed in the 3-D strain space that accounts for the gradual accumulation of both plastic strains and damage

Training Opportunities: Co-Organizer: Symposium "Advances in Multiscale-Modeling of the Effect of Anisotropy in Forming" at Numisheet 2018, the 11th International Conference and Workshop on Numerical Simulation of 3D Sheet Metal Forming Processes (MS-5): <http://numisheet2018.org/Mini-Symposiums/index.html>, July 30-August 3, 2018, Tokyo, Japan (with Dr. N. Chandola, Univ. of Florida/REEF).

Co-Organizer: Symposium "Anisotropic Plasticity of Textured and Microstructurally Heterogeneous Materials" at IMECE 2018 ASME International Mechanical Engineering Congress and Exposition, November 9-15, 2018, Pittsburgh, Pennsylvania, USA (with Dr. H. Eliot Fang, Sandia National Laboratories)

Chair: ICACM 2017, The 10th US-France Symposium "Dynamic Damage and Fragmentation" 17-19 May 2017, Shalimar, FL, http://www.reef.ufl.edu/ICACM_website/publication.html.

PIs organized: Symposium "Titanium: Constitutive Modeling and Numerical Simulations of Forming Processes" Numisheet 2016, the 10th International Conference and Workshop on Numerical Simulations of 3D Sheet Forming Processes 4-9 September 2016, Bristol, United Kingdom

RPPR Final Report

as of 16-Sep-2019

Results Dissemination: Monograph:

O. Cazacu, B. Revil-Baudard, N. Chandola [2019] Plasticity-Damage Couplings: From Single Crystal to Polycrystalline Materials, Springer, 2019; 518 pp., <https://doi.org/10.1017/978-3-319-92922-4> , ISBN 978-3-319-92921-7 (<https://www.springer.com/gb/book/9783319929217>)

Book Chapter:

J.L. Alves and O. Cazacu [2017] Effect of the third-invariant of the stress deviator on the response of porous solids with pressure-insensitive matrix, Chapter 5 in: From microstructure investigations to multiscale modeling : bridging the gap", Wiley-ISTE, 2017, Eds: S. Bouvier, D.Brancherie, P. Feisel, A. Ibrahimegovic Wiley-ISTE, 2017, ISBN: 978-1-78630-259-5.

Refereed Journal Publications

1. O. Cazacu and B. Revil-Baudard [2016] New analytic criterion for porous solids with pressure-insensitive matrix, Int. J. Plasticity, 89, 66-84.
2. O. Cazacu [2018]. New yield criteria for isotropic and textured metallic materials. International Journal of Solids and Structures, 139, 200-210.
3. B. Revil-Baudard, O. Cazacu, N. Chandola [2018] Effect of the ratio between the yield stresses in uniaxial tension and pure shear on the shape and size of the plastic zone near a crack , Int. J. Plasticity, 102, 101-117.
4. D. Savage, N. Chandola, O. Cazacu, Brandon A. McWilliams, Marko Knezevic [2018] Validation of recent analytical dilatational models for porous polycrystals using crystal plasticity finite element models with Schmid and non-Schmid activation laws (2018), Mechanics of Materials 126, 148-162.

LECTURES PRESENTED AT PROFESSIONAL CONFERENCES/MEETINGS

International Conferences

- 1.O. Cazacu [2018] "On modeling plastic anisotropy: From single-crystal to polycrystal" Keynote Lecture, 2018 Int. Plasticity Symposium, San Juan, PR, USA, Jan. 3-8, 2018.
- 2.O. Cazacu, N. Chandola, B. Revil-Baudard [2018] "Prediction of plastic anisotropy in yield stresses and Lankford coefficients of textured polycrystalline sheets using a new single-crystal yield criterion" Invited Talk, 21th International Conference on Metal Forming, ESAFORM 2018, April 23-25, 2018, Palermo, Italy.
- 3.O. Cazacu [2018] "New yield criteria for isotropic and textured metals" Invited Talk, 10th European Solid Mechanics Conference, ESMC 2018, July 2-6, 2018, Bologna, Italy.
- 4.O. Cazacu, B. Revil-Baudard [2017] "Coupled effects of second and third invariants on void growth and collapse, Invited Talk, 2017 ASME International Mechanical Engineering Congress and Exposition, November 3-9, 2017, Tampa, Florida, USA.
- 5.O. Cazacu, J.L. Alves [2017] "Role of Intrinsic Plastic Deformation Mechanisms on the Rate of Damage Accumulation under Cyclic Loadings" 2017 ASME International Mechanical Engineering Congress and Exposition, November 3-9, 2017, Tampa, Florida, USA.
- 6.O. Cazacu "Constitutive modeling of plastic deformation and damage in anisotropic high-purity titanium and validation using ex-situ and in-situ tomography data" Keynote Lecture, Numisheet 2016, the 10th International Conference and Workshop on Numerical Simulations of 3D Sheet Forming Processes 4-9 September 2016, Bristol, UK.
- 7.O. Cazacu [2016] "Role of the matrix plastic flow on the mechanical response of porous solids", Invited Talk, ICTAM 2016, August 21-26, Montreal, Canada.
8. O. Cazacu [2016] "New analytic criterion for porous solids with pressure-insensitive matrix governed by an yield criterion involving the third-invariant of the stress deviator", 21st European Conference of Fracture, June 20-24, Catania, Italy.
- 9.O. Cazacu [2016] The key role played by the matrix plastic flow on the rate of void growth and collapse in polycrystalline metals", Invited Lecture, ICACM 2016 symposium, June 1-3, Compiègne, France.

RPPR Final Report

as of 16-Sep-2019

Honors and Awards: Honors and Awards

- University Carlos III Madrid, Spain, Chair of Excellence Professorship (2018-2020) in recognition of outstanding research in solid mechanics
- University of Florida Term Professorship (2017-2020) in recognition of excellence in teaching, research, and service
- University of Lorraine, Metz, France, Visiting Fellowship (1 month 2018) in recognition of excellence research in dynamic plasticity and failure
- Appointed: Deputy Editor of Plasticity Book Series, Elsevier (since July, 2018)
- Appointed: Associate Editor, Mechanics Research Communication, Elsevier, <https://www.journals.elsevier.com/mechanics-research-communications> (since June 2018)
- Appointed: Associate Editor, International Journal of Material Forming, Springer <https://www.springer.com/engineering/industrial+management/journal/12289> (since December, 2017).

Protocol Activity Status:

Technology Transfer: • Transitioned algorithms for implementation into Lagrangian DoD code EPIC code of criterion developed by the PI; the POC: Dr. Gordon Johnson Southwest Research Institute.

- Dr. Brandon A. McWilliams, U.S. Army Research Laboratory, Aberdeen, MD : collaboration that resulted in one journal publication (see list of publications issued from the research reported)
- Dr. Joel Stewart, U.S. Army Research Laboratory Aberdeen, MD: research interactions concerning damage modeling

PARTICIPANTS:

Participant Type: PD/PI

Participant: Oana Cazacu

Person Months Worked: 5.00

Funding Support:

Project Contribution:

International Collaboration:

International Travel:

National Academy Member: N

Other Collaborators:

Participant Type: Co PD/PI

Participant: Benoit Revil-Baudard

Person Months Worked: 5.00

Funding Support:

Project Contribution:

International Collaboration:

International Travel:

National Academy Member: N

Other Collaborators:

Participant Type: Postdoctoral (scholar, fellow or other postdoctoral position)

Participant: Nitin Chandola

Person Months Worked: 11.00

Funding Support:

Project Contribution:

International Collaboration:

International Travel:

National Academy Member: N

Other Collaborators:

Participant Type: Graduate Student (research assistant)

Participant: Hernan Godoy

Person Months Worked: 14.00

Funding Support:

Project Contribution:

International Collaboration:

RPPR Final Report

as of 16-Sep-2019

International Travel:
National Academy Member: N
Other Collaborators:

ARTICLES:

Publication Type: Journal Article Peer Reviewed: Y **Publication Status:** 1-Published

Journal: Mechanics of Materials

Publication Identifier Type: DOI

Publication Identifier: 10.1016/j.mechmat.2018.08.004

Volume: 126

Issue:

First Page #: 148

Date Submitted: 8/30/19 12:00AM

Date Published: 8/18/18 5:00AM

Publication Location: United States

Article Title: Validation of recent analytical dilatational models for porous polycrystals using crystal plasticity finite element models with Schmid and non-Schmid activation laws

Authors: Daniel Savage, Nitin Chandola, Oana Cazacu, Brandon A. McWilliams, Marko Knezevic

Keywords: Voided polycrystals; Crystal plasticity; Non-Schmid effects; Analytic criteria for porous materials; Void evolution; Tension-compression asymmetry

Abstract: Recent analytic criteria for isotropic porous materials developed by (Cazacu et al., 2013) revealed the importance of considering specificities of plastic behavior in the matrix. On one hand it was shown that if the matrix material is governed by the von Mises criterion, the yield surface of the porous material should be centrosymmetric and, with the exception of hydrostatic and purely deviatoric loadings, there are combined effects of the mean stress and third-invariant of the stress deviator on void growth or collapse; but on the other hand if the matrix plastic deformation displays strength differential (SD) effects, the response is also sensitive to third-invariant and there is a lack of symmetry of the yield surface of the porous material. In this paper, we use a unit cell modeling approach in conjunction with a crystal plasticity finite element model to verify these theoretical predictions. The resulting numerical points representing the homogenized yield surfaces and void growth

Distribution Statement: 1-Approved for public release; distribution is unlimited.

Acknowledged Federal Support: Y

BOOKS:

Publication Type: Book Peer Reviewed: Y **Publication Status:** 1-Published

Publication Identifier Type: DOI

Publication Identifier: <https://doi.org/10.1017/978-3-319-92922-4>

Book Edition: 1

Volume:

Publication Year: 2019

Date Received: 22-Aug-2018

Publication Location: Cham, Switzerland

Publisher: Springer

Book Title: Plasticity-damage couplings: From Single Crystal to Polycrystalline Materials

Authors: Oana Cazacu, Benoit Revil-Baudard, Nitin Chandola

Editor:

Acknowledged Federal Support: Y

CONFERENCE PAPERS:

Publication Type: Conference Paper or Presentation

Publication Status: 1-Published

Conference Name: Numisheet 2018

Date Received: 22-Aug-2018

Conference Date: 30-Jul-2018

Date Published: 07-Aug-2018

Conference Location: Tokyo, Japan

Paper Title: Anisotropic yield criteria

Authors: Oana Cazacu

Acknowledged Federal Support: Y

RPPR Final Report
as of 16-Sep-2019

Final Report

Grant # W911NF-16-1-0159

1.2. Solid Mechanics

Period of Performance: 4/12/2016-04/13/2019

Uncovering the cause of ratcheting and low cycle fatigue

PI: Dr. Oana Cazacu, Co-PI: Dr. Benoit Revil-Baudard
Department of Mechanical and Aerospace Engineering,
University of Florida, REEF, Shalimar, FL 32579, USA.
cazacu@reef.ufl.edu; revil@ufl.edu

Submitted to:

Dr. Denise Ford

Program Manager Solid Mechanics

Denise.c.ford2.civ@mail.mil

and

Dr. Ralph A. Anthenien Jr

Chief, Mechanical Sciences Division Army Research Office

ralph.a.anthenien2.civ@mail.mil

P.O. Box 12211 Research Triangle Park,

NC 27709-2211

Abstract

The project focused on the development of a novel modeling framework for low cycle fatigue under multiaxial loadings, with special emphasis on providing understanding of the manner in which the specificities of the plastic deformation influence crack propagation. Key accomplishments have been achieved: a) we developed a new potential for isotropic materials which is expressed in the three-dimensional strains space and accounts for gradual accumulation of both plastic strains and damage, b) we addressed the question of the role of the Lode parameter on damage evolution, and discovered what is the relative weight of the invariants in the matrix for which this parameter has either maximum influence or no influence on damage evolution, c) we developed new elastic solutions for the stresses and strains in the vicinity of cracks that better describe the near-tip behavior and do not violate the boundary conditions on the surface of the crack, d) we developed new analytical relations between the external loading and the size of the plastic zone that accounts for yielding characteristics, e) we developed a new potential accounting for plastic anisotropy that it is expected to further assist in understanding the role of anisotropy on fatigue crack growth rate. The grant has also greatly facilitated the writing by the investigators of the monograph "Plasticity-Damage couplings from single-crystal to polycrystalline materials" which was recently published by Springer Nature <https://www.springer.com/gb/book/9783319929217> .

1. Introduction

Models and fatigue life relations are based on stress, strain, or energy parameters. The strain-based models are more appropriate for description of low cycle fatigue (LCF) behavior (see Fekete, 2015). However these formulations are predominantly one-dimensional (e.g. Coffin, 1974; Murakami et al. 2005; Surajit et al. 2010; Zhang et al. 2013; Li et al., 2014; Lefebvre et al., 1984) with the value of certain parameters being made dependent on whether the loading is axial or torsional (e.g. the exponent in the Coffin-Manson relation (see Coffin, 1974)). Three-dimensional (3-D) fatigue models have been proposed, but those are expressed in stresses. As pointed out by Chaboche et al (2012), none of these models predict with accuracy fatigue behavior under cyclic torsion or more complex multi-axial loadings (e.g. for biaxial conditions involving combined shear and axial loadings, see Taleb and Cailletaud, 2010).

One of the objectives of the project was to develop a novel potential expressed in the 3-D strain space that accounts for the gradual accumulation of both plastic strains and damage. Most

importantly, using this potential for the first time it was established that depending on the relative weight of the invariants in the matrix the effect of the Lode parameter on damage evolution can be completely erased. The key findings are summarized in Section 2 while full mathematical proofs and discussion is given in the paper issued from this research of Cazacu and Revil-Baudard (2017).

Beginning with the seminal studies of fatigue service of Paris and collaborators, it is well accepted that the rate of crack propagation is related to the stress intensity factor, as is the plastic zone. While significant progress has been made in development of experimental techniques for small-scale testing that enable improved accuracy in the measurement of the plastic zone for engineering structural materials, there is still a critical need for finding how the particularities of yielding influence the size of the plastic zone that develops around cracks. Another objective of the project was to investigate this open problem. Key discoveries were made. Specifically, we obtained new elastic solutions for the stresses and strains in the vicinity of cracks that better describe the near-tip behavior and do not violate the boundary conditions on the surface of the crack a new elastic solution (see Section 3). This new elastic solution made possible further advancements in solving the long-standing problem of determining the extent of the plastic zone in front of a crack in a thin sheet subject to uniaxial tension. For the first time, it was established a correlation between the extent of the plastic zone and the ratio between the yield stresses in simple tension and pure shear. This in turn allows explaining the experimentally observed differences in terms of plastic zone sizes between engineering materials. Moreover, new analytic relations for the length of the plastic zone, measured from the crack tip in the crack plane, and the external applied load were established for the case when yielding is governed by the von Mises and Tresca criteria, respectively. These new results are summarized in Section 4 and more details can be found in the paper of Revil-Baudard et al (2018) issued as a result of this investigation.

The influence of plastic anisotropy of materials on fatigue life remains a major concern. Key in advancing the understanding is an appropriate representation of the material symmetries induced by the fabrication process (e.g. transverse isotropy induced by extrusion; orthotropy induced by rolling). A new anisotropic plastic potential was developed in the framework of the theory of representation of tensor functions (Cazacu, 2018). This potential and its predictive capabilities are summarized in Section 4. Finally, the grant has greatly facilitated the writing by the

investigators of the monograph "Plasticity-Damage couplings from single-crystal to polycrystalline materials" very recently published by Springer Nature <https://www.springer.com/gb/book/9783319929217> .

2. Cazacu and Revil-Baudard (2017) plastic potential

To address the question concerning what should be the relative weight of the invariants in the matrix for which we have the maximum influence or erase completely the effect of Lode parameter a two-step approach was adopted. Namely, we proposed a new isotropic model for fully-dense materials that depends on both invariants, $\psi_{CB}(\mathbf{d})$, and then we developed an analytic criterion for porous materials with matrix behavior governed by this potential $\psi_{CB}(\mathbf{d})$.

While the isotropic plastic potential for fully-dense materials developed and its properties are discussed in detail in Cazacu and Revil (2017) here we present only the main equations. This isotropic strain-rate potential (SRP) is expressed as:

$$\psi_{CB}(\mathbf{d}) = \frac{\sqrt{j_2}}{B} \left(1 + \beta \frac{j_3^2}{j_2^3} \right), \quad (1)$$

with

$$B = \frac{1 + 4\beta/27}{\sqrt{4/3}} . \quad (2)$$

In Eq.(1), $j_2 = (\mathbf{d}:\mathbf{d})/2$ is the second-invariant of the plastic strain-rate tensor \mathbf{d} , $j_3 = \det(\mathbf{d})$ is the third-invariant of \mathbf{d} , whereas β is a parameter of the model. The constant B appearing in the expression of the criterion depends solely on β and it is defined such that for uniaxial tension $\psi_{CB}(\mathbf{d})$ is equal to the axial strain rate. Let us recall that for $\psi_{CB}(\mathbf{d})$ to be convex, the range of variation of β is,

$$\frac{-9}{24} \leq \beta \leq \frac{27}{68} . \quad (3)$$

Most importantly, depending on the sign of the parameter β , this isotropic SRP is either interior to the von Mises strain-rate potential ($\beta < 0$), coincides with it ($\beta = 0$), or it is exterior to it

($\beta > 0$). On the other hand, irrespective of the value of β , Tresca's potential $\psi_{Tresca}(\mathbf{d})$ is an upper-bound for $\psi_{CB}(\mathbf{d})$.

To arrive at a closed-form expression of the plastic potential for the porous material with matrix described by $\psi_{CB}(\mathbf{d})$ (see Eq.(1)), we conducted limit analysis on a hollow sphere subjected to axisymmetric loadings and made use of the Rice and Tracey (1969) velocity field. It was shown that it is possible to solve the limit analysis problem analytically, and to obtain the plastic dissipation of the damaged material $\Pi_{CB}^+(\mathbf{D}, f)$, where \mathbf{D} is the macroscopic strain-rate tensor and f is a measure of damage (void volume fraction). As a consequence, the strain-rate potential of the damaged material, $\Psi_{CB}^+(\mathbf{D}, f) = \Pi_{CB}^+(\mathbf{D}, f) / \sigma_T$ can be obtained in closed-form. Moreover, we derived an explicit analytic expression of the yield criterion for the damaged material, namely:

$$\left\{ \begin{array}{l} \Sigma_m / \sigma_T = \frac{1}{3} \frac{\partial \Psi_{CB}^+(\mathbf{D}, f)}{\partial D_m} \\ \Sigma_e / \sigma_T = \left| \frac{\partial \Psi_{CB}^+(\mathbf{D}, f)}{\partial D_e} \right| \end{array} \right. , \quad (4)$$

where D_m and D_e denote the first-invariant and the second-invariant of the macroscopic strain-rate tensor \mathbf{D} , respectively. It is worth noting that the potential of the damaged material, $\Psi_{CB}^+(\mathbf{D}, f)$, needs to be calculated only for loadings such that ($D_m \geq 0, D'_{11} > 0$) and ($D_m \geq 0, D'_{11} < 0$), respectively.

In the following, we present only the key steps of the proof and the parametric representation of the yield surface of the damaged material. For more details, the reader is referred to the referenced paper of Cazacu and Revil-Baudard (2017).

Theorem 1 (Strain-rate potential for porous materials with matrix depending on both invariants)

For axisymmetric states, the strain-rate potential of the porous material is given by:

- a) For $D_m \geq 0$ and $J_3^D \leq 0$ ($D'_{11} \geq 0$), irrespective of the value of $u = 2|D_m| / D_e$:

$$\Psi_{CB}^+(\mathbf{D}, f) = \frac{\sqrt{3}uD_e}{4B} \left(H_1\left(\frac{u}{f}\right) - H_1(u) \right), \quad (5)$$

with

$$\begin{aligned} H_1(y) &= -\frac{2\sqrt{3}}{3} \beta \tan^{-1}\left(\frac{2y-1}{\sqrt{3}}\right) \\ &+ \frac{2\sqrt{3}}{9} \left(1 + \frac{11}{3}\beta\right) \left(\tan^{-1}(\sqrt{3} + 2\sqrt{y}) - \tan^{-1}(-\sqrt{3} + 2\sqrt{y})\right) \\ &+ \left(\frac{9y^{3/2} + \sqrt{3} - 3y\sqrt{3} - 3y^2\sqrt{3}}{9y^{3/2}} - \beta \frac{6y^2\sqrt{3} + 9y^{3/2} - 12y\sqrt{3} - 2\sqrt{3}}{27y^{3/2}} \right) \ln(-\sqrt{3}y + y + 1) \\ &- \frac{4}{3y} + \frac{4\beta(4y^2 - 4y + 1)}{27(y^2 - y + 1)y} + \frac{13}{27}\beta \ln(y^2 - y + 1) \\ &+ \left(\frac{9y^{3/2} + 3y\sqrt{3} + 3y^2\sqrt{3} - \sqrt{3}}{9y^{3/2}} + \beta \frac{-12y\sqrt{3} + 6y^2\sqrt{3} - 9y^{3/2} - 2\sqrt{3}}{27y^{3/2}} \right) \ln(\sqrt{3}y + y + 1) \end{aligned} \quad (6)$$

b) $D_m \geq 0$ and $J_3^D \geq 0$ ($D'_{11} \leq 0$),

$$\Psi^+(\mathbf{D}, f) = \begin{cases} \frac{\sqrt{3}uD_e}{4B} \left(A_1\left(\frac{u}{f}\right) - A_1(u) \right), & \forall u < f \\ \frac{\sqrt{3}uD_e}{4B} \beta \left(-\frac{7}{27}\pi - \frac{4\sqrt{3}}{27}\ln(3) + \frac{4\sqrt{3}}{9} \right), & \forall f < u < 1 \\ \frac{\sqrt{3}uD_e}{4B} \left(A_2\left(\frac{u}{f}\right) - A_2(u) \right), & \forall u > 1 \end{cases} \quad (7)$$

with $A_1(u)$ and $A_2(u)$ given by:

$$\begin{aligned}
A_1(y) = & -\frac{2\beta}{\sqrt{3}} \tan^{-1}\left(\frac{2y+1}{\sqrt{3}}\right) - \frac{2\sqrt{3}}{27}(3+11\beta) \left(\begin{array}{c} \tan^{-1}\left(\frac{2\sqrt{y}-1}{\sqrt{3}}\right) \\ -\tan^{-1}\left(\frac{2\sqrt{y+1}}{\sqrt{3}}\right) \end{array} \right) \\
& - \frac{2\sqrt{3}}{9y^{3/2}} \left(3y^2 - 3y - 1 + \frac{2\beta}{3}(3y^2 + 6y - 1) \right) \tan^{-1}\left(\frac{\sqrt{3y}}{y-1}\right) \\
& - \frac{(4\beta+27)}{27} \ln(y^2 + y + 1) + \left(\frac{4\beta(4y^2 + 4y + 1) - 9(y^2 + y + 1)}{27y(y^2 + y + 1)} \right),
\end{aligned} \tag{8}$$

and

$$\begin{aligned}
A_2(y) = & -\frac{2}{\sqrt{3}} \beta \tan^{-1}\left(\frac{2y+1}{\sqrt{3}}\right) \\
& + \frac{2\sqrt{3}}{27}(3+11\beta) \left(\tan^{-1}\left(\frac{2\sqrt{y}-1}{\sqrt{3}}\right) - \tan^{-1}\left(\frac{2\sqrt{y+1}}{\sqrt{3}}\right) \right) \\
& + \frac{2\sqrt{3}}{9y^{3/2}} \left(3y^2 - 3y - 1 + \frac{2\beta}{3}(3y^2 - 1 + 6y) \right) \tan^{-1}\left(\frac{\sqrt{3y}}{y-1}\right) \\
& + \frac{27+4\beta}{27} \ln(y^2 + y + 1) - \frac{4\beta(4y^2 + 4y + 1) - 9y - 9 - 9y^2}{27y(y^2 + y + 1)}.
\end{aligned} \tag{9}$$

Proofs:

Case (a) : For $D_m \geq 0$ and $J_3^D \leq 0$ ($D'_{11} \geq 0$) :

$$\begin{aligned}
\frac{B}{\sqrt{3}} \Psi_{CB}(\mathbf{d}) = & \sqrt{D_m^2 (b/r)^6 + D'_{11} D_m (b/r)^3 (3 \cos^2 \theta - 1) + D'_{11}{}^2} \\
& + \beta \frac{\left(D_m (b/r)^3 + D'_{11} \right)^2 \left(2D_m^2 (b/r)^6 + D_m D'_{11} (b/r)^3 (9 \cos^2 \theta - 5) + 2D'_{11}{}^2 \right)^2}{27 \left(D_m^2 (b/r)^6 + D_m D'_{11} (b/r)^3 (3 \cos^2 \theta - 1) + D'_{11}{}^2 \right)^{5/2}}
\end{aligned} \tag{10}$$

Since for the applied loading, the strain-rate triaxiality $u = 2D_m / D_e = D_m / D'_{11}$ using the change of variable $y = u(b/r)^3$ and $\alpha = \cos \theta$ in the integral representing $\Psi_{CB}^+(\mathbf{D}, f)$, we obtain:

$$\frac{4B}{\sqrt{3}} \Psi_{CB}^+(\mathbf{D}, f) = (uD_e) \int_u^{u/f} \int_{-1}^1 \left(\frac{\sqrt{y^2 + (3\alpha^2 - 1)y + 1}}{y^2} + \frac{\beta (y+1)^2 (2y^2 + (9\alpha^2 - 5)y + 2)^2}{27 (y^2 + (3\alpha^2 - 1)y + 1)^{5/2}} \right) dy d\alpha \quad (11)$$

Further integration with respect to y leads to the expression given in Eq.(5). Furthermore, for

($D_m \geq 0$ and $D'_{11} \geq 0$) from Eq.(11), it follows that: $\frac{\partial \Psi_{CB}^+(\mathbf{D}, f)}{\partial D_{11}} \geq \frac{\partial \Psi_{CB}^+(\mathbf{D}, f)}{\partial D_{33}}$ and

$\frac{\partial \Psi_{CB}^+(\mathbf{D}, f)}{\partial D_m} \geq 0$, so the stresses at yielding of the porous material are such that the third-

invariant of the stress deviator $J_3^\Sigma = -2(\Sigma_{11} - \Sigma_{33})^3 / 27$ is negative, and the mean stress $\Sigma_m \geq 0$.

For all other loading scenarios, the analysis can be conducted in a similar way. Therefore, we obtain the following result:

Theorem 2: The parametric representation of the yield surface of a damaged material with matrix described by the model depending on both invariants given by Eq. (1) is:

a) For $\Sigma_m \geq 0$ and $J_3^\Sigma \leq 0$ and any value of $u = 2|D_m| / D_e$:

$$\begin{cases} \Sigma_m / \sigma_T = \frac{2}{3} \frac{\sqrt{3}u^2}{4B} \left(H_1(u/f) - H_1(u) + u \left(\frac{1}{f} H_1'(u/f) - H_1'(u) \right) \right) \\ \Sigma_e / \sigma_T = -\frac{\sqrt{3}u^2}{4B} \left(\frac{1}{f} H_1'(u/f) - H_1'(u) \right) \end{cases} \quad (12)$$

where the prime symbol denoted the first derivative of the function $H_1(y)$ given by Eq.(6)

b) For stress states such that $\Sigma_m \geq 0$ and $J_3^\Sigma \geq 0$, the yield surface of the porous material is:

- For $u < f$:

$$\begin{cases} \Sigma_m / \sigma_T = \frac{2}{3} \frac{\sqrt{3}u^2}{4B} \left(A_1(u/f) - A_1(u) + u \left(\frac{1}{f} A_1'(u/f) - A_1'(u) \right) \right) \\ \Sigma_e / \sigma_T = -\frac{\sqrt{3}u^2}{4B} \left(\frac{1}{f} A_1'(u/f) - A_1'(u) \right) \end{cases} \quad (13)$$

- For $f < u < 1$:

$$\left\{ \begin{array}{l} \Sigma_m / \sigma_T = \frac{2\sqrt{3}u^2}{3\ 4B} \left(A_2(u/f) - A_1(u) + \beta \left(-\frac{7}{27}\pi - \frac{4\sqrt{3}}{27}\ln(3) + \frac{4\sqrt{3}}{9} \right) - \right. \\ \left. \sqrt{3}\ln(3) - \frac{4\sqrt{3}}{3} + \frac{\pi}{9} + u \left(\frac{1}{f} A_1'(u/f) - A_1'(u) \right) \right) \\ \Sigma_e / \sigma_T = -\frac{\sqrt{3}u^2}{4B} \left(\frac{1}{f} A_1'(u/f) - A_2'(u) \right) \end{array} \right. \quad (14)$$

- For $u > 1$:

$$\left\{ \begin{array}{l} \Sigma_m / \sigma_T = \frac{2\sqrt{3}u^2}{3\ 4B} \left(A_2(u/f) - A_2(u) + (u/f)A_2'(u/f) - uA_2'(u) \right) \\ \Sigma_e / \sigma_T = -\frac{\sqrt{3}u^2}{4B} \left(\frac{1}{f} A_2'(u/f) - A_2'(u) \right) \end{array} \right. \quad (15)$$

where $A_1'(y)$ and $A_2'(y)$ denote the first derivatives of the functions $A_1(y)$ and $A_2(y)$, respectively which are given by Eq.(8) and Eq.(9). For $\Sigma_m \leq 0$ and $J_3^\Sigma \geq 0$, the parametric representation of the yield surface of the damaged material is obtained from Eq. (12) by arguments of centro-symmetry.

- c) Similarly, for loadings such $\Sigma_m \leq 0$ and $J_3^\Sigma \leq 0$, the parametric representation of the yield surface of the porous solid is obtained from Eqs. (13)-(15).

Remarks:

It is important to note that in developing the SRP (see Theorem 1) and the yield criterion for the damaged material (see Theorem 2), no approximations were made when calculating the local plastic dissipation. Neglecting, the cross-term $D_m D'_{11}$ involved in the expression of $\psi_{CB}(\mathbf{d})$ (for example, see Eq.(11)) would have resulted in erasing the specificities of the plastic deformation of the matrix, and as such the resulting yield criterion of the porous solid would have been independent of the third-invariant J_3^Σ or Lode parameter. For $\beta = 0$, the Cazacu and Revil-Baudard (2017) criterion reduces to the Cazacu et al. (2013) criterion for porous Mises material. Irrespective of the value of the parameter β , it is predicted that yielding of the porous material has the following properties:

- The absolute value of the yield limit under hydrostatic tensile loadings is the same as the yield limit under purely hydrostatic compression loadings: $-2/3\sigma_T \ln f$.

- For purely deviatoric axisymmetric loadings, yielding occurs at $\Sigma_e = \sigma_T(1-f)$, irrespective of the sign of J_3^Σ .

The above properties are a direct consequence of the plastic potential of the matrix being an even function (see Eq.(1)).

2.1. Effect of the matrix sensitivity to both invariants on yielding

On the basis of the analytic criterion for isotropic porous materials (see Theorem 2 and respective equations) it is possible to draw general conclusions pertaining to the role played by the matrix sensitivity to both invariants of plastic deformation. In the following analysis, we will take advantage of the fact that, irrespective of the value of the parameter β , the yield surface of the porous solid is centro-symmetric. Therefore, we will represent and analyze only the quadrant of the yield surface defined by (Σ_e, Σ_m) with $\Sigma_m \geq 0$. We recall that for axisymmetric loadings with $\Sigma_{11} = \Sigma_{22}$, the equivalent stress Σ_e reduces to $|\Sigma_{11} - \Sigma_{33}|$, the mean stress is: $\Sigma_m = (2\Sigma_{11} + \Sigma_{33})/3$, and the third-invariant of the stress deviator is: $J_3^\Sigma = -2(\Sigma_{11} - \Sigma_{33})^3 / 27$.

In Figure 1 are represented for the same level of porosity ($f = 5\%$), the yield surfaces corresponding to materials with matrix characterized by $\beta = 0.38$, 0, (von Mises matrix), $\beta = -0.15$ and $\beta = -0.35$, respectively. It is very interesting to note that if the matrix is characterized by $\beta \geq 0$ i.e. its plastic potential is exterior or coincides with von Mises (see also Section 6.1.1.3), the response of the porous material for loadings such that $\Sigma_{11} = \Sigma_{22} \leq \Sigma_{33}$ (i.e. at $J_3^\Sigma \geq 0$) is softer than that for loadings such that $\Sigma_{11} = \Sigma_{22} \geq \Sigma_{33}$ (i.e. at $J_3^\Sigma \leq 0$), the yield curve corresponding to $J_3^\Sigma \geq 0$ is below that corresponding to $J_3^\Sigma \leq 0$. The stronger is the sensitivity of the matrix plastic deformation to the third-invariant (i.e. the larger the value of β in Eq.(1)), the stronger is the influence of J_3^Σ on yielding of the porous material.

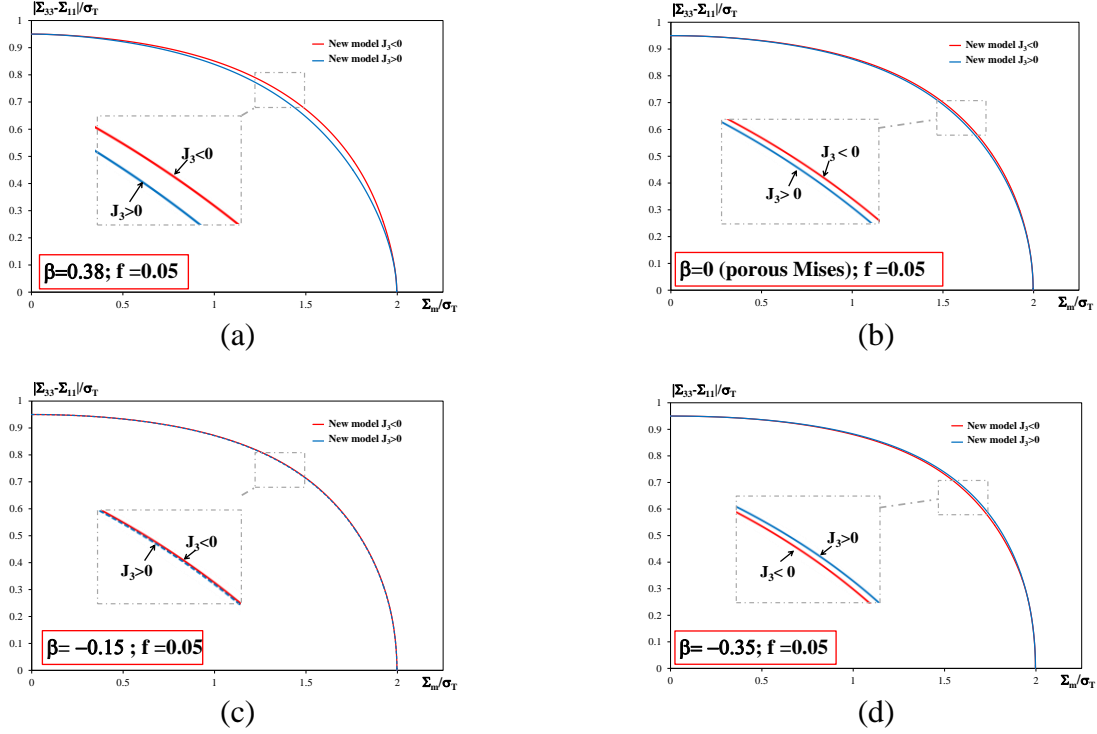


Figure 1. Effect of the third-invariant J_3^Σ on yielding of porous materials with matrix characterized by: (a) $\beta = 0.38$; (b) $\beta = 0$ (von Mises matrix); (c) $\beta = -0.15$; (d) $\beta = -0.35$. Porosity $f = 5\%$ for all materials.

It is also very interesting to note that for the material with matrix characterized by $\beta = -0.15$ and porosity $f = 5\%$ there is practically no influence of J_3^Σ on the behavior (see Figure 1(c) showing that the yield curve corresponding to $J_3^\Sigma \leq 0$ almost coincides with the one that corresponds to $J_3^\Sigma \geq 0$). It means that although the matrix behavior depends on both invariants, the presence of voids practically erases the influence of J_3^Σ on yielding of the porous material. The same conclusion, i.e. practically no influence of J_3^Σ on the response applies to a material characterized by a porosity $f = 1\%$ and matrix with $\beta = -0.15$ (see Figure 2(b)). It is to be noted that the particular value of β , say β_* , for which the porous material has no influence on the third-invariant can be determined.

For fixed values of the porosity f , ranging from 10^{-5} to 0.15 , we obtain:
 $-0.179 < \beta_* < -0.172$.

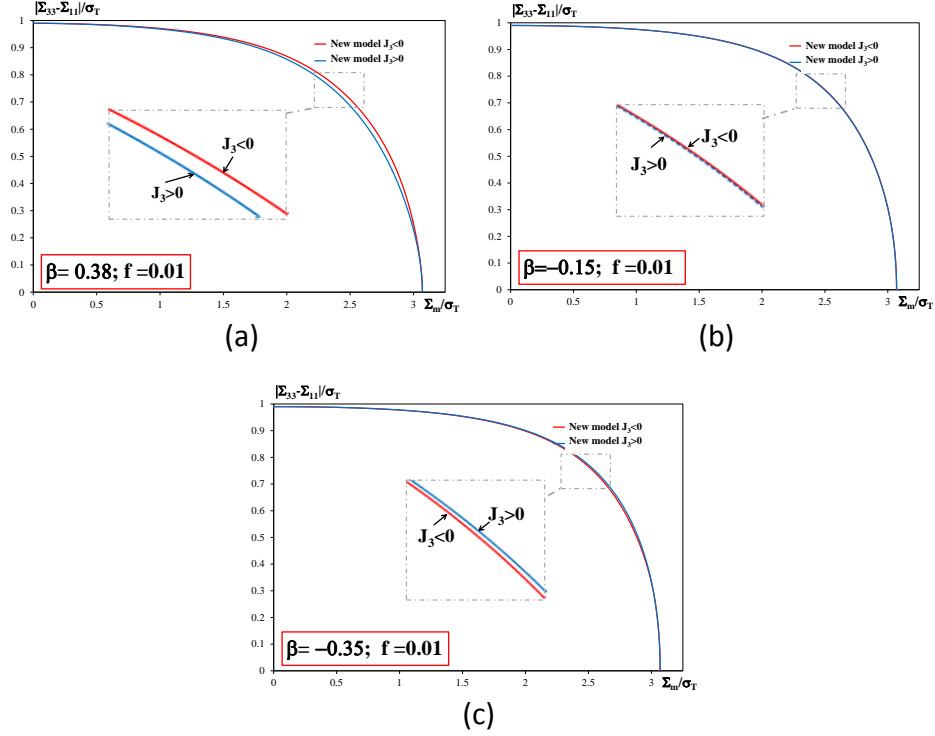


Figure 2. Effect of the third-invariant J_3^Σ on yielding of porous materials with matrix characterized by: (a) $\beta = 0.38$; (b) $\beta = -0.15$; (c) $\beta = -0.35$. For all materials, $f = 1\%$.

It is also worth comparing the yield surfaces of porous materials according to Cazacu and Revil-Baudard (2017) with the yield surface of a porous Tresca material obtained using the Cazacu et al. (2014c) criterion. For axisymmetric loadings $\Sigma_{11} = \Sigma_{22} \leq \Sigma_{33}$ (i.e. at $J_3^\Sigma \geq 0$) the respective surfaces for $f = 5\%$ are shown in Figure 3; for loadings corresponding to $\Sigma_{11} = \Sigma_{22} \geq \Sigma_{33}$ (i.e. at $J_3^\Sigma \leq 0$), the respective surfaces are shown in Figure 4. It is very interesting to note that irrespective of the imposed loading, if the matrix is characterized by $\beta > 0$, the yield surface of the porous material lies between the yield surface of a porous von Mises material and the yield surface of a porous Tresca material. Specifically, for $\beta > 0$ the porous Tresca yield surface is a lower bound while the porous von Mises surface is an upper bound. Moreover, the stronger the deviation of the matrix behavior from von Mises (i.e. the larger the value of β in Eq.(1), the closer is the yield surface is to that of a porous Tresca material.

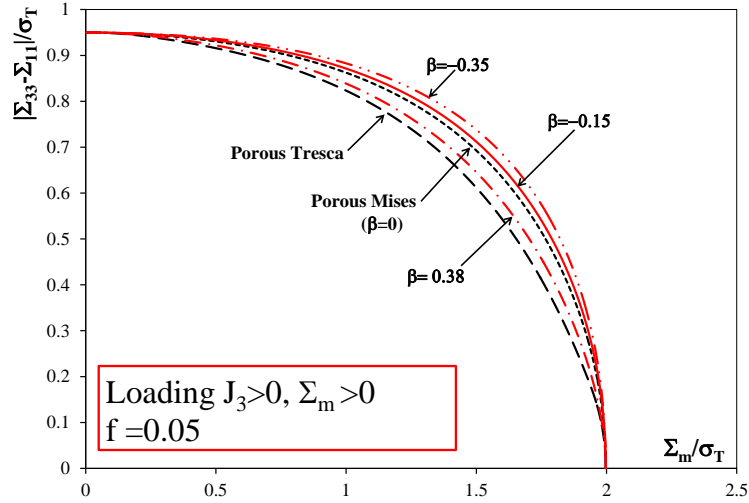


Figure 3. Comparison between the yield surfaces of a porous Mises material ($\beta = 0$), a porous Tresca material according to the Cazacu et al. (2014c) criterion and those of porous materials with matrix characterized by $\beta = 0.38$, $\beta = -0.15$, $\beta = -0.35$, respectively, calculated with the Cazacu and Revil-Baudard (2017) criterion for axisymmetric loadings such that $J_3^\Sigma \geq 0$ ($\Sigma_{11} = \Sigma_{22} \leq \Sigma_{33}$).

On the other hand, the response of the porous material with von Mises matrix ($\beta = 0$) is softer than that of a porous material with matrix characterized by $\beta < 0$. The smaller the value of β , the more pronounced is the difference in response as compared to that of a porous von Mises material.

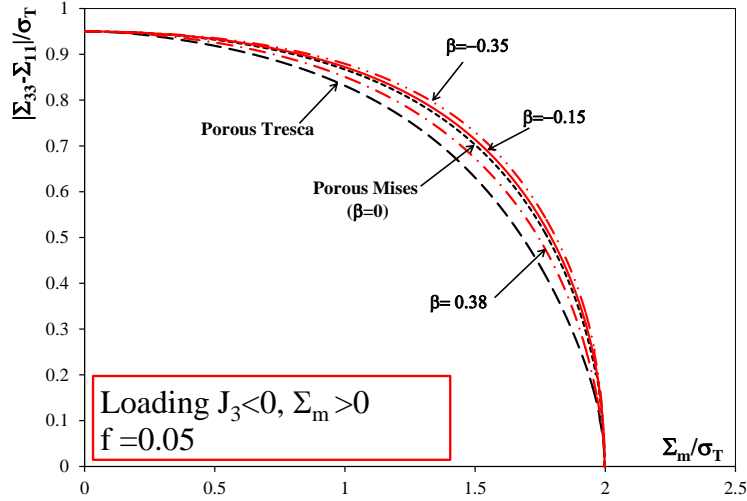


Figure 4. Comparison between the yield surfaces of a porous Mises material ($\beta = 0$), a porous Tresca material according to the Cazacu et al. (2014c) criterion and those of porous materials with matrix characterized by $\beta = 0.38$, $\beta = -0.15$, $\beta = -0.35$, respectively, calculated with the Cazacu and Revil-Baudard (2017) criterion for axisymmetric loadings such that $J_3^\Sigma \leq 0$ ($\Sigma_{11} = \Sigma_{22} \geq \Sigma_{33}$).

As expected, the yield limit for purely deviatoric states and purely hydrostatic states is the same for all porous materials irrespective of the criterion governing the plastic deformation of the matrix (see also Theorem 2).

2.2. Influence of the matrix sensitivity to both invariants on damage evolution

We have shown that the value of the parameter β which describes the relative weighting of the invariants on the plastic deformation of the matrix strongly affects the rate of void evolution. As an example, in Figure 5 are compared the predictions of the void growth versus the overall equivalent plastic strain E_e corresponding to porous materials with a matrix characterized by $\beta = 0.38$, $\beta = -0.15$, and $\beta = -0.35$ which were subjected to axisymmetric loadings at fixed stress triaxiality $T = 1.5$ with either $\Sigma_{11} = \Sigma_{22} < \Sigma_{33}$ (i.e. at $J_3^\Sigma \geq 0$) or $\Sigma_{11} = \Sigma_{22} > \Sigma_{33}$ (i.e. at $J_3^\Sigma < 0$). For all porous materials considered the initial porosity was $f_0 = 0.5\%$.

It is very interesting to note that for the material characterized by a matrix with a value of $\beta = -0.15$, close to β_* , the rate of void growth for loadings such that $J_3^\Sigma \geq 0$ and $J_3^\Sigma \leq 0$, respectively are almost the same (see Figure 5(b)). This is consistent with the fact that for the

same material there is practically no effect of J_3^Σ on yielding (see Figure 2(b)). On the other hand, if the matrix is characterized by $\beta > \beta_*$, the rate of void growth is faster for loadings such that $J_3^\Sigma \geq 0$ than for loadings at $J_3^\Sigma \leq 0$; and the larger is the value of β , the stronger is the effect of J_3^Σ on void growth. On the contrary, if the matrix is characterized by $\beta < \beta_*$, the rate of void growth is faster for $J_3^\Sigma \leq 0$ than for $J_3^\Sigma \geq 0$ (see for example, Figure 5(c) which presents the void evolution for the material with matrix characterized by $\beta = -0.35$). Since the criterion is centrosymmetric, the following conclusions can be drawn concerning the effect of the matrix plastic deformation on void collapse (i.e. void evolution for compressive mean stress):

- If the porous solid has the matrix characterized by $\beta > \beta_*$, the rate of void collapse is faster for loadings at $J_3^\Sigma \leq 0$ than for loadings at $J_3^\Sigma \geq 0$;
- If the porous solid has the matrix characterized by β close to β_* , there is practically no effect of J_3^Σ on void collapse;
- If the porous solid has the matrix characterized by a value of the parameter $\beta < \beta_*$ the rate of void collapse is faster for loadings at $J_3^\Sigma \geq 0$ than for loadings at $J_3^\Sigma \leq 0$.

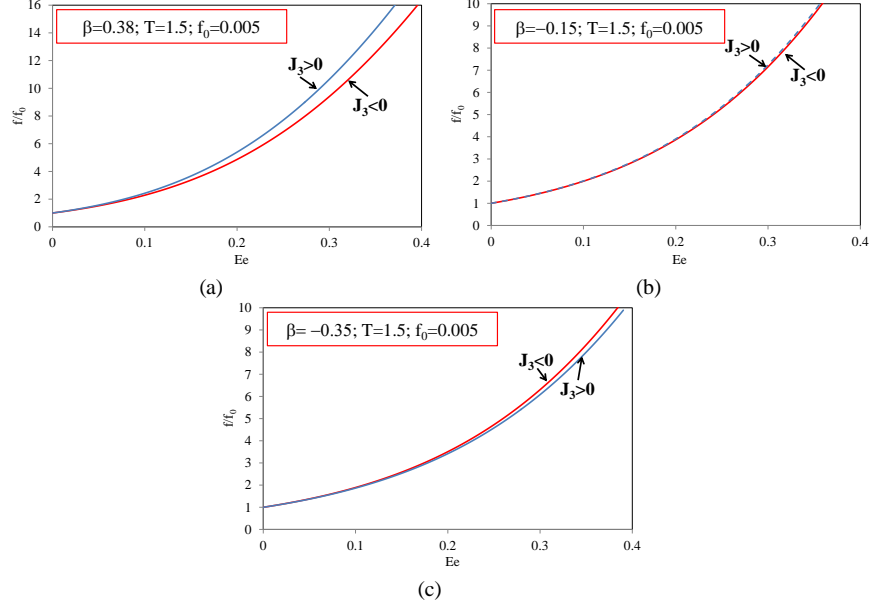


Figure 5. Effect of the third-invariant J_3^Σ on the void volume fraction (f/f_0) evolution with the overall equivalent plastic strain for axisymmetric loadings at fixed triaxiality $T=1.5$ predicted by the Cazacu and Revil-Baudard (2017) criterion for porous materials characterized by matrix with (a) $\beta = 0.38$; (b) $\beta = -0.15$; (c) $\beta = -0.35$. For all materials the initial porosity is: $f_0 = 0.5\%$.

It is also worth comparing the void growth rates and collapse with that of a porous Tresca material. Let us first consider a porous material with matrix characterized by $\beta = -0.15$ (close to $\beta_* = -0.175$). Note that the void growth and void closure rates in this porous material are slower than in both a porous von Mises material and a porous Tresca material, respectively (see Figure 6 and Figure 7). In contrast to both Tresca and von Mises porous materials, for this porous material there is practically no effect of J_3^Σ on void evolution.

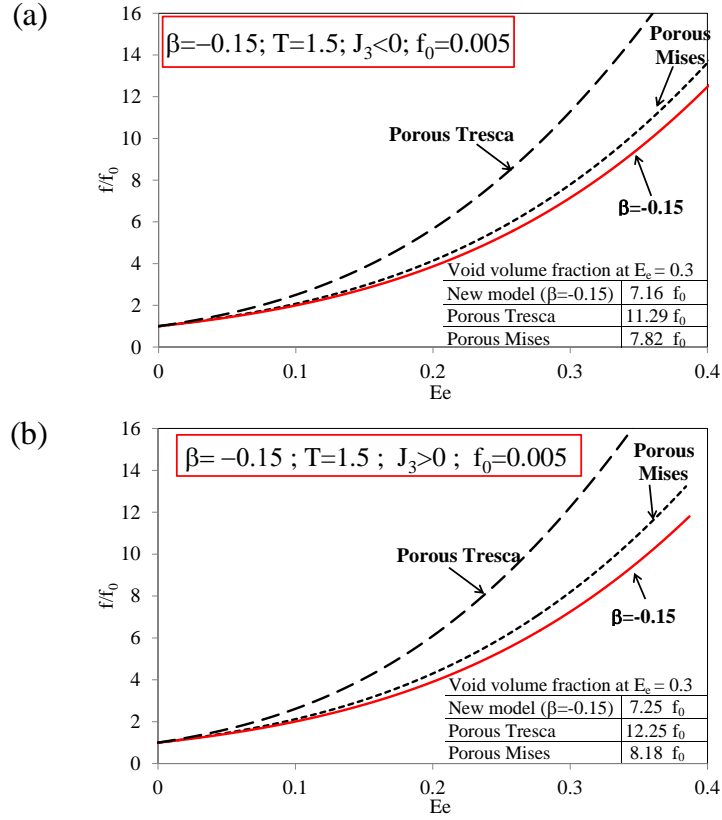


Figure 6. Comparison between the evolution of the void volume fraction with the overall equivalent plastic strain E_e for axisymmetric loadings at fixed stress-triaxiality $T = 1.5$ for a porous von Mises material (according to Cazacu et al. (2013)), a porous Tresca material (using Cazacu et al. (2014c)) and for porous solids with matrix characterized by $\beta = -0.15$ according to the Cazacu and Revil-Baudard (2017) criterion: (a) axisymmetric loadings such that $J_3^{\Sigma} \leq 0$ and (b) axisymmetric loadings such that $J_3^{\Sigma} \geq 0$. For the porous material with $\beta = -0.15$ there is practically no influence of J_3^{Σ} on void growth.

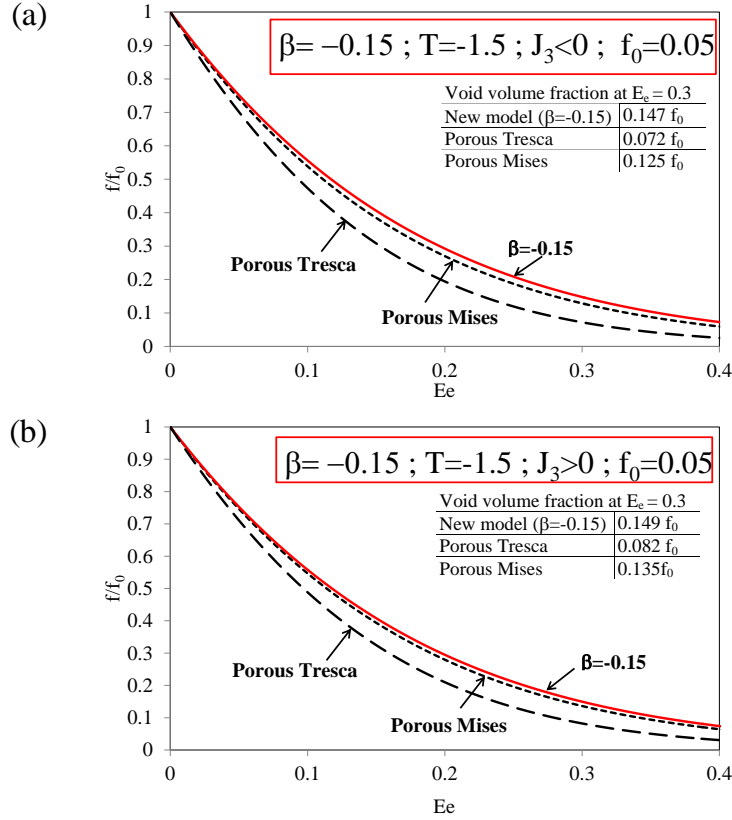


Figure 7. Comparison between the evolution of the void volume fraction with the overall equivalent plastic strain E_e for compressive axisymmetric loadings at fixed stress triaxiality $T = 1.5$ for a porous von Mises material (according to Cazacu et al. (2013)), a porous Tresca material (using Cazacu et al. (2014c)) and for a porous material with matrix characterized by $\beta = -0.15$ (a) axisymmetric loadings such that $J_3^{\Sigma} \leq 0$ and (b) axisymmetric loadings such that $J_3^{\Sigma} \geq 0$; Initial porosity $f_0 = 0.05$. For the porous material with $\beta = -0.15$ there is practically no influence of J_3^{Σ} on void collapse.

On the other hand, if the matrix is characterized by $\beta > 0 > \beta_*$, the relative weight of the invariants on the matrix behavior is such that irrespective of the type of loading (i.e. sign of J_3^{Σ}), the rate of void growth is faster than in a porous von Mises material ($\beta = 0$) and lower than in a porous Tresca material. As an example, in Figure 8 and Figure 9 is presented the evolution of the void volume fraction f/f_0 with the overall effective plastic strain for a porous material with matrix characterized by $\beta = 0.38$ subjected to axisymmetric loading histories corresponding to either ($J_3^{\Sigma} \leq 0$) or ($J_3^{\Sigma} \geq 0$) and fixed positive stress triaxiality $T = 1.5$. The initial void volume

fraction is $f_0 = 0.5\%$. For example, for axisymmetric loadings such that $J_3^\Sigma \leq 0$, at an equivalent plastic strain of $E_e = 0.3$, the void volume fraction is $f = 7.82f_0$ in the porous Mises material, $9.41f_0$ in the material with matrix characterized by $\beta = 0.38$, against $11.29f_0$ in the porous Tresca material.

While for all porous materials the rate of void growth is faster for axisymmetric loadings such that $J_3^\Sigma \geq 0$ (see Figure 8(b)) than for axisymmetric loadings such that $J_3^\Sigma \leq 0$ (see Figure 8(a)), the maximum influence of J_3^Σ on void evolution is displayed by the material characterized by $\beta = 0.38$. For example at $E_e = 0.3$, in this material the difference between the porosity attained in loadings with $J_3^\Sigma \leq 0$ and $J_3^\Sigma \geq 0$ is of 13% while for the porous Tresca material the difference is of 8%, and for the porous Mises material there is 5% difference. The same conclusions can be drawn from the analysis of the void evolution in a porous material with matrix characterized by $\beta = 0.2$. However, the influence of J_3^Σ on void growth is less pronounced. As an example, at $E_e = 0.3$, the difference between the porosity attained in loadings corresponding to $J_3^\Sigma \leq 0$ and $J_3^\Sigma \geq 0$ is of 13% for the material with matrix characterized by $\beta = 0.38$ against 9.5% for the one corresponding to a matrix with $\beta = 0.2$ and only 5% for a material with matrix characterized by $\beta = 0$ (von Mises matrix). In general, for $\beta > \beta_*$ the influence of J_3^Σ on void growth is less pronounced as the value of the parameter β decreases.

Since both the Cazacu and Revil-Baudard (2017) criterion and the Cazacu et al. (2014c) criterion for a porous Tresca material display centro-symmetry, the same effects of the relative weighting of the invariants in the matrix (i.e. of β) on the rate of void collapse should occur. Comparisons between the predictions of void collapse as a function of the overall effective strain for axisymmetric loadings at fixed compressive triaxiality $T = -1.5$ corresponding to either $J_3^\Sigma \leq 0$ or $J_3^\Sigma \geq 0$ are shown in Figure 9. The initial porosity was considered higher ($f_0 = 5\%$) such as to allow a larger range of plastic strain to develop prior to void closure. Irrespective of the sign of the third invariant, the rate of void closure in the material with matrix characterized by $\beta = 0.38$ is much faster than in the porous Mises material, and only slightly slower than the rate of void

closure in the porous material with Tresca matrix (see Figure 9(a) for $J_3^\Sigma \leq 0$ and Figure 9(b) for $J_3^\Sigma \geq 0$). While for all porous materials the rate of void closure is faster for axisymmetric loadings such that $J_3^\Sigma \leq 0$ than for axisymmetric loadings such that $J_3^\Sigma \geq 0$, the influence of J_3^Σ on the rate of void collapse is more pronounced for the material with matrix characterized by $\beta = 0.38$ (18% difference between $J_3^\Sigma \leq 0$ and $J_3^\Sigma \geq 0$ at $E_e = 0.3$) than for the porous Tresca material (13 % difference at $E_e = 0.3$) and the porous Mises material (8 % difference at $E_e = 0.3$). The same conclusions can be drawn by analyzing the rate of void closure in a porous material with matrix characterized by $\beta = 0.2$ as compared to that in the porous von Mises and porous Tresca material, respectively. However, the influence of J_3^Σ on the rate of void collapse is less pronounced than in the case when the matrix is characterized by $\beta = 0.38$. As an example, at $E_e = 0.3$, the difference between the porosity corresponding to loadings at $J_3^\Sigma \leq 0$ and $J_3^\Sigma \geq 0$ is of 18% for the material with matrix characterized by $\beta = 0.38$, against 12% for the material characterized by $\beta = 0.2$ and 8% for the material with $\beta = 0$ (porous Mises solid). As already mentioned, if the matrix is characterized by $\beta > \beta_*$, the influence of J_3^Σ on void evolution decreases as the value of the parameter β decreases.

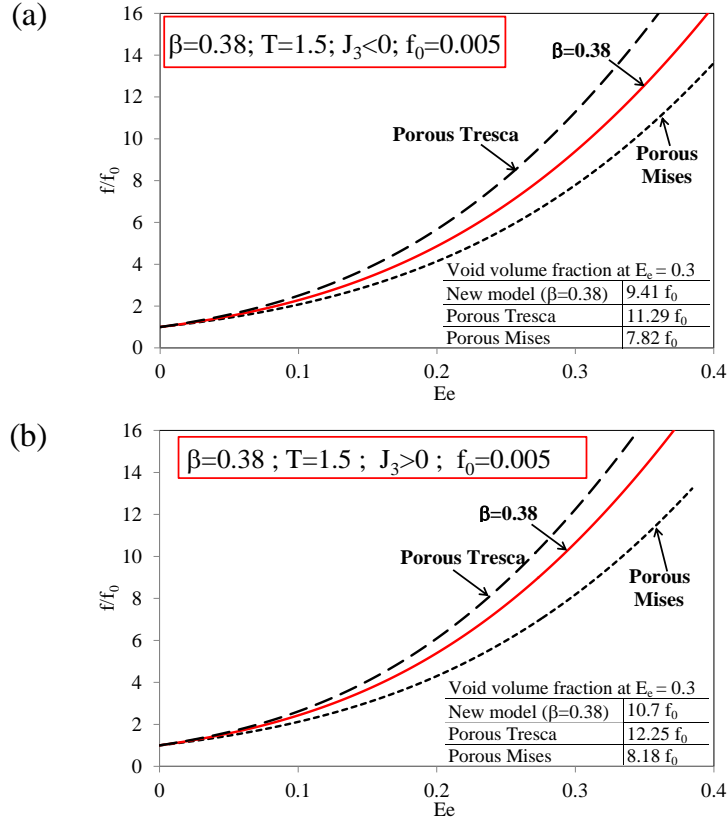


Figure 8. Comparison between the evolution of the void volume fraction with equivalent plastic strain E_e for axisymmetric loadings at fixed stress triaxiality $T = 1.5$ for a porous von Mises material according to Cazacu et al. (2013) criterion, a porous Tresca material according to Cazacu et al. (2014c) and a porous material with matrix characterized by $\beta = 0.38$ (a) axisymmetric loadings such that $J_3^{\Sigma} \leq 0$ and (b) axisymmetric loadings such that $J_3^{\Sigma} \geq 0$; Initial porosity $f_0 = 0.5\%$.

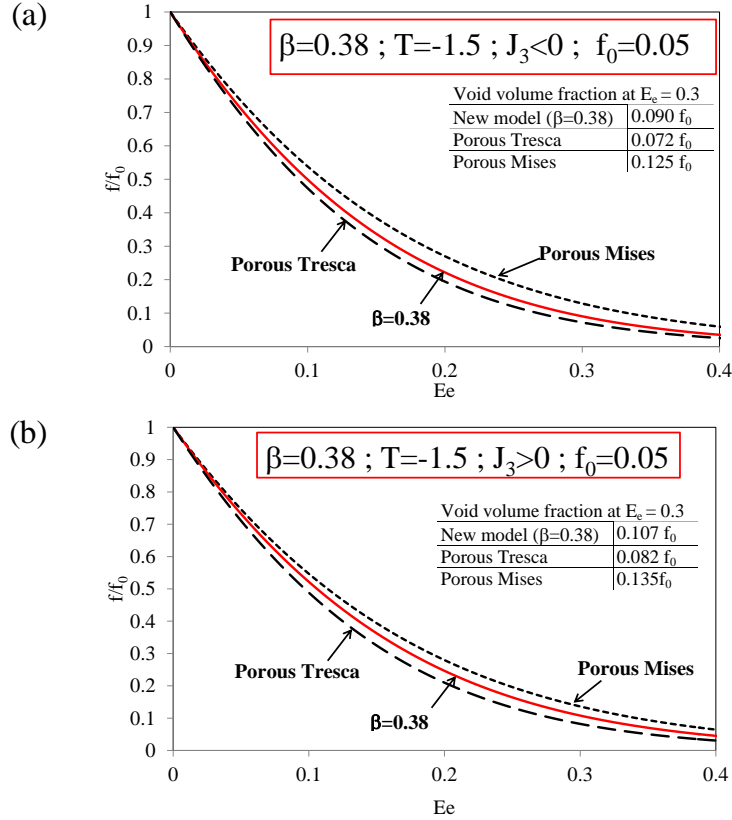


Figure 9. Comparison between the evolution of the void volume fraction with equivalent plastic strain E_e for axisymmetric loadings at fixed stress triaxiality $T = -1.5$ for a porous von Mises material according to the Cazacu et al. (2013) criterion, a porous Tresca material according to the Cazacu et al. (2014c) and a porous material with matrix characterized by $\beta = 0.38$ (a) axisymmetric loadings such that $J_3^\Sigma \leq 0$ and (b) axisymmetric loadings such that $J_3^\Sigma \geq 0$; Initial porosity $f_0 = 5\%$

In summary, for stress triaxialities T different from zero or infinity the response of the porous Tresca material is softer than that of the porous von Mises material which in turn is softer than that of a porous material with matrix characterized by $\beta < 0$ (see also Figure 3 and Figure 4). As a consequence, in porous materials with $\beta < 0$, the rate of void growth and the rate of void closure will be slower than the rate of void evolution in a porous Mises material and a porous Tresca material, respectively. As an example, let us examine Figure 10(a) which shows the void growth evolution with the overall effective strain E_e in a porous material with matrix characterized by $\beta = -0.35$ subjected to axisymmetric tensile loadings at a fixed stress

triaxiality $T = 1.5$. Note that for axisymmetric loadings such that $J_3^\Sigma \leq 0$, at $E_e = 0.3$ in the porous material with $\beta = -0.35$, the void volume fraction is $f = 6.30f_0$, against $f = 11.3f_0$ in the porous Tresca material, and $f = 7.82f_0$ in the porous Mises material ($\beta = 0$). It is also worth noting that while for the porous Mises and porous Tresca materials, the void growth rate is faster for loadings at $J_3^\Sigma \geq 0$ than for loadings at $J_3^\Sigma \leq 0$, for the material with matrix characterized by $\beta = -0.35$, the reverse occurs i.e. the void growth rate is slower for loadings at $J_3^\Sigma \geq 0$ than for loadings at $J_3^\Sigma \leq 0$. Due to the centro-symmetry of all criteria, it follows that the void closure rate will also be slower than in a porous von Mises material. The same conclusions, i.e. that the void closure rate will be faster for $J_3^\Sigma \geq 0$ than for $J_3^\Sigma \leq 0$ can be drawn for any porous material with matrix characterized by $\beta < \beta_*$ (see Figure 11).

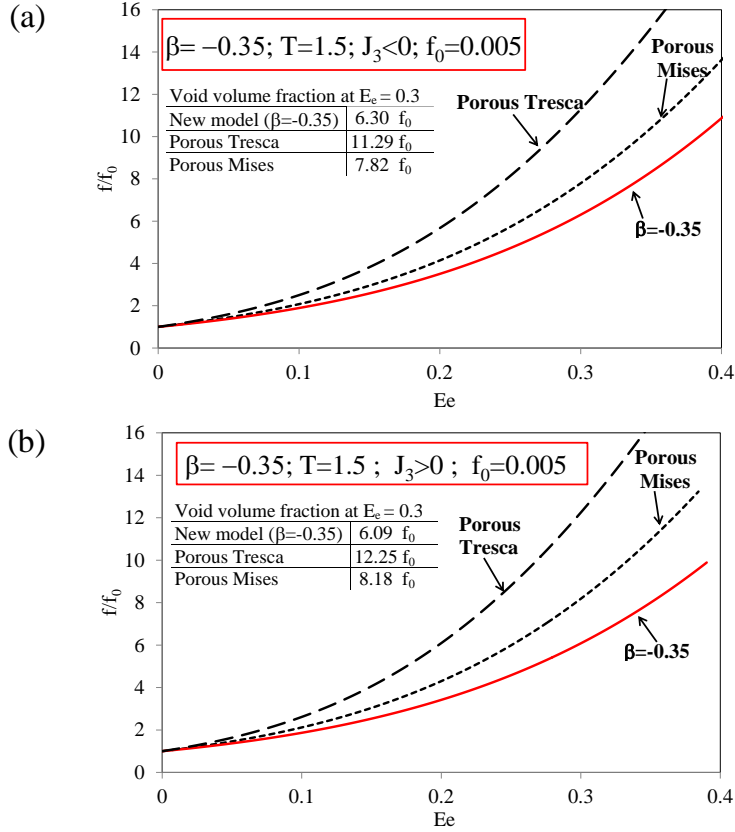


Figure 10. Comparison between the evolution of the void volume fraction with equivalent plastic strain E_e for axisymmetric loadings at fixed stress triaxiality $T = 1.5$ for a porous von Mises material (according to Cazacu et al. (2013)), a porous Tresca material (using Cazacu et al. (2014c)) and a porous material with matrix characterized by $\beta = -0.35$: (a) axisymmetric loadings such that $J_3^x \leq 0$ and (b) axisymmetric loadings such that $J_3^x \geq 0$; Initial porosity $f_0 = 0.5\%$

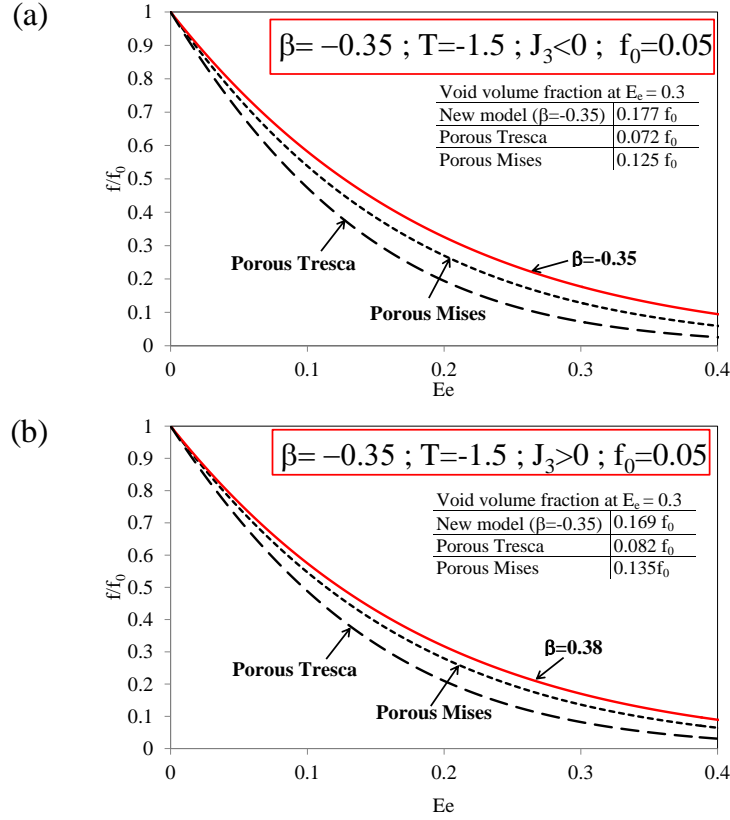


Figure 11. Comparison between the evolution of the void volume fraction with equivalent plastic strain E_e under compressive axisymmetric loadings at fixed stress triaxiality $T = -1.5$ for a porous von Mises material according to Cazacu et al. (2013) criterion, a porous Tresca material (according to Cazacu et al. (2014c)) and a porous material with matrix characterized by $\beta = -0.35$: (a) axisymmetric loadings such that $J_3^{\Sigma} \leq 0$ and (b) axisymmetric loadings such that $J_3^{\Sigma} \geq 0$; Initial porosity $f_0 = 5\%$

In summary, it was established that:

- A porous material with matrix governed by Tresca criterion has the fastest rate of void growth or collapse.
- However, depending on the specific dependence of the matrix plastic deformation to the invariants of the stress deviator, the rate of void growth or collapse in a porous material can be either faster or slower than that of a porous Mises material. Specifically,
- If the matrix is characterized by $\beta > 0$, the void growth rate is faster than in a porous Mises material; the larger is the value of β , the faster is the rate of void evolution, which approaches the one in a porous Tresca material.

- If the matrix is characterized by $\beta < 0$, the rate of void growth and the rate of void closure are slower than in a porous Mises material. The smaller is the value of β , the slower is the rate of void growth as compared to a von Mises porous material.

3. Influence of the yielding characteristics on the size of the plastic zone near a crack in a thin sheet loaded in tension

3.1. Statement of the problem and determination of the elastic stress field

Let us consider a thin plate having a center crack of length $2a$ and subjected to uniaxial tension. Let Oxy a Cartesian system with the origin at the center of the plate, the x -axis (or \mathbf{e}_x) directed along the crack and the y -axis (or \mathbf{e}_y) along the loading direction. The boundary of the crack is traction free. Since in practice, the crack length is much smaller than any in-plane linear dimension, the boundary conditions of the problem are:

$$\sigma_{xx} = \sigma_{xy} = 0 \text{ at } |x| \leq a \text{ and } y = 0;$$

$$\sigma_{yy} = S \text{ and } \sigma_{xx} = \sigma_{xy} = 0 \text{ at infinity.} \quad (16)$$

For an applied load S sufficiently small, the material response is elastic obeying the classic Hooke's law. In the elastic regime, finding the solution to the problem reduces to determination of the Airy stress function ϕ satisfying the biharmonic equation:

$$\nabla^4 \phi = 0. \quad (17)$$

The stress components are given by:

$$\begin{aligned}
\sigma_{xx} &= \frac{\partial^2 \phi}{\partial y^2} \\
\sigma_{yy} &= \frac{\partial^2 \phi}{\partial x^2} \\
\sigma_{xy} &= -\frac{\partial^2 \phi}{\partial y \partial x}.
\end{aligned} \tag{18}$$

Westergaard (1939) derived the following complex potential that satisfies the biharmonic equation (Eq. (17)) :

$$\phi(z) = \frac{Sz}{\sqrt{z^2 - a^2}}, \tag{19}$$

with $z = x + iy$, and \bar{z} its complex conjugate. This is the potential that is generally used to obtain the near crack-tip solution of the elastic stress field (e.g. see the monograph by Sun and Jin (2012)). Namely, substitution of Eq.(19) into Eq.(18) leads to the following elastic stress field:

$$\sigma_{xx} = \sigma_{yy} \text{ and } \sigma_{xy} = 0 \quad \text{at } y = 0, \tag{20}$$

and the near crack-tip solution:

$$\sigma_{xx} = \sigma_{yy} = \frac{S\sqrt{\pi a}}{\sqrt{2\pi r}}, \quad \sigma_{xy} = 0, \tag{21}$$

with r being the distance to the crack tip. As pointed out by Westergaard (1939), this stress field is axisymmetric, therefore it does not satisfy the boundary conditions of the problem. If the applied load is sufficiently large, plastic strains will develop at some location near the crack tip where the yield condition is first satisfied. Since the elastic stress field given by Eq.(21) is axisymmetric, all isotropic yield criteria predict the same critical level of the applied load and the same extent of the plastic zone near the crack tip.

As mentioned, as part of the project we obtained the exact elastic solution to the biharmonic equation with boundary conditions given by Eq.(16) (see Revil-Baudard et al., 2018). For this purpose, we solved the associated problem of determining the state of stress around an elliptic

hole of semi-axes a and b (see Fig. 12). Note that when b is very small the corresponding ellipse is very slender, and in the limit $b \approx 0$, it becomes a crack. For the purpose of understanding the key differences between this solution and the classic stress field of Westergaard (1939) that is customarily used in the literature, in the following we present the approach, and the main steps in the derivation of the exact solution. For the detailed proof the reader is referred to Revil-Baudard and Cazacu (2018).

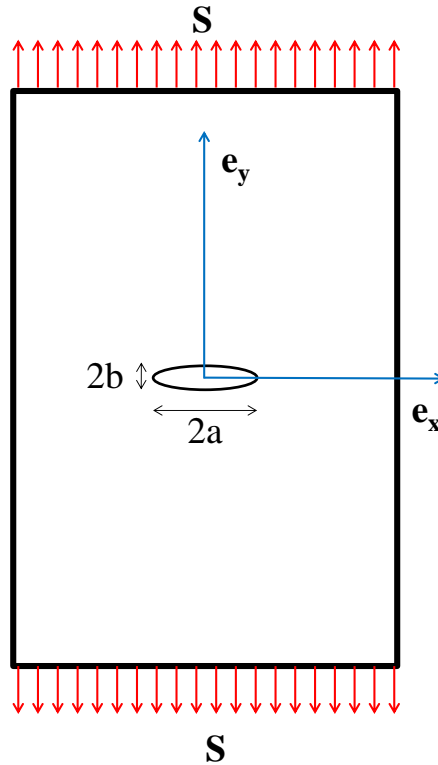


Figure 12: Description of the problem of a thin plate having a center crack of length $2a$ subjected to uniaxial tension S .

Given the geometry of the problem, it is advantageous to consider the elliptical coordinates (ξ, η) (see Figure 13) such that:

$$\begin{cases} x = c \cosh(\xi) \cos(\eta) \\ y = c \sinh(\xi) \sin(\eta) \end{cases} \quad (22)$$

Thus,

$$z = x + iy = c \cosh(\zeta) \quad \text{with} \quad \zeta = \xi + i\eta \quad \text{and} \quad c = \sqrt{a^2 - b^2}. \quad (23)$$

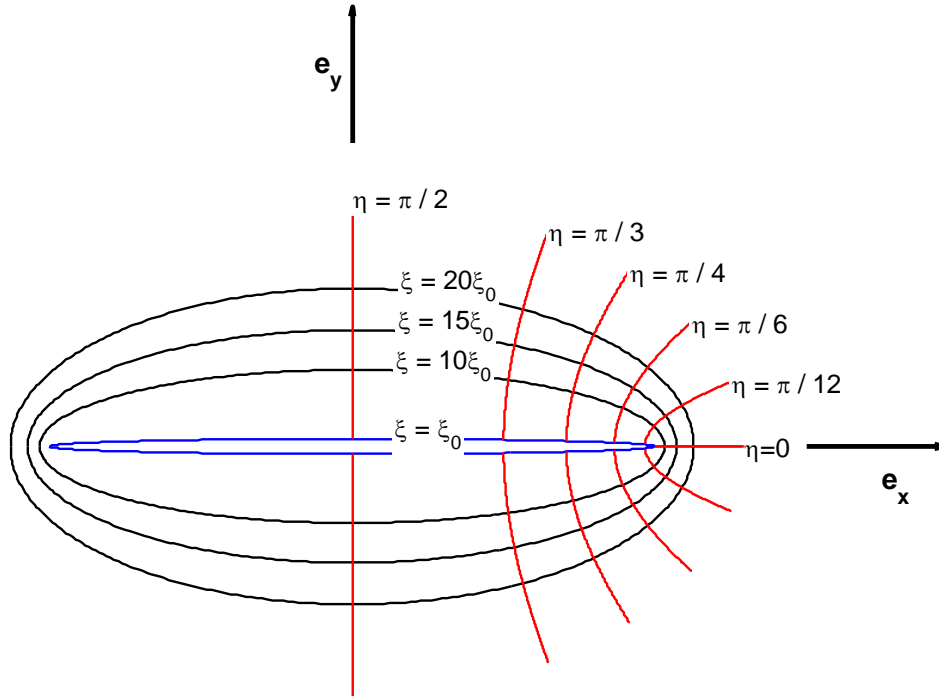


Figure 13: Definition of the curvilinear elliptical coordinates (ξ, η) .

Note that the boundary of the hole corresponds to:

$$\xi = \xi_0 \quad \text{and} \quad \eta \in [0, 2\pi], \quad \text{with} \quad \tanh(\xi_0) = b/a. \quad (24)$$

The state of stress is specified by $\sigma_{\xi\xi}$, the normal stress component on a curve $\xi = \text{constant}$, $\sigma_{\eta\eta}$ the normal stress component on a curve $\eta = \text{constant}$, and $\sigma_{\xi\eta}$ the shear stress component on both curves (see Fig. 24). Using the Cauchy-Riemann equations, it can be shown that the solution to the biharmonic equation (17) is expressible as:

$$\phi(z, \bar{z}) = \text{Re}(\bar{z}\psi(z) + \chi(z)). \quad (25)$$

Therefore, finding the solution reduces to the determination of the functions $\psi(z)$ and $\chi(z)$.

Once these functions are known, further use of Eq.(18) leads to:

$$\begin{cases} \sigma_{\xi\xi} + \sigma_{\eta\eta} = 4 \operatorname{Re}(\psi'(z)) \\ \sigma_{\eta\eta} - \sigma_{\xi\xi} + 2i\sigma_{\xi\eta} = 2 \frac{\sinh(\zeta)}{\sinh(\bar{\zeta})} [\bar{z}\psi''(z) + \chi''(z)]. \end{cases} \quad (26)$$

Given the geometry of the problem, Stevenson (1945) proposed that the potentials $\psi(z)$ and $\chi(z)$ should be taken of the general form:

$$\begin{aligned} \psi(\zeta) &= c [A \cosh(\zeta) + B \sinh(\zeta)] \\ \chi(\zeta) &= c^2 [\zeta + D \cosh(2\zeta) + E \sinh(2\zeta)], \end{aligned} \quad (27)$$

with A, B, C, D, E being real numbers. By imposing the boundary conditions (see Eq.(24)),

the following solution for the elastic stresses around an elliptic hole in a plate subject to uniaxial tension S in a direction at right angle to the major axis is obtained:

$$\sigma_{\eta\eta} = \frac{Se^{2\xi_0}}{2} \left[\begin{aligned} & -1 + \frac{(1 + e^{-2\xi_0}) \sinh(2\xi)}{(\cosh(2\xi) - \cos 2\eta)^2} (\cosh(2\xi) + \cosh(2\xi_0) - 2 \cos 2\eta) \\ & + \frac{\cosh(2\xi - 2\xi_0) \cos 2\eta - \cosh(2\xi_0)}{\cosh(2\xi) - \cos 2\eta} \end{aligned} \right] \quad (28)$$

$$\sigma_{\xi\xi} = -\sigma_{\eta\eta} + Se^{2\xi_0} \left[-1 + \frac{(1 + e^{-2\xi_0}) \sinh(2\xi)}{\cosh(2\xi) - \cos 2\eta} \right] \quad (29)$$

$$\sigma_{\xi\eta} = Se^{2\xi_0} \frac{\sin(2\eta) \sinh(\xi - \xi_0)}{(\cosh(2\xi) - \cos 2\eta)^2} \left[(1 + e^{-2\xi_0}) \sinh(\xi + \xi_0) + (\cosh(2\xi) - \cos 2\eta) \cosh(\xi - \xi_0) \right] \quad (30)$$

It can be easily verified that this solution fulfills the boundary conditions, i.e.:

- $\sigma_{yy} = S$ and $\sigma_{xx} = \sigma_{xy} = 0$ (uniaxial tension) at large distances from the hole ($\xi \rightarrow \infty$)
- $\sigma_{\xi\eta} = \sigma_{\xi\xi} = 0$ on the elliptical boundary of the hole, i.e. for $\xi = \xi_0$ and $\eta \in [0, 2\pi]$.

It is worth noting that the axial stress at the crack tip in the crack plane is:

$$\sigma_{yy} \Big|_{x=a, y=0} = \sigma_{\eta\eta} \Big|_{\xi=\xi_0, \eta=0}.$$

According to Eq.(28), the stress $\sigma_{\eta\eta}$ at the boundary of the hole (i.e. $\xi = \xi_0$, see also Fig. 23) is:

$$\left(\sigma_{\eta\eta}\right)_{\xi=\xi_0} = S e^{2\xi_0} \left[-1 + \frac{(1 + e^{-2\xi_0}) \sinh(2\xi)}{\cosh(2\xi_0) - \cos 2\eta} \right], \quad (31)$$

Thus, $\left(\sigma_{\eta\eta}\right)_{\xi=\xi_0}$ attains its maximum value at the tip of the hole, i.e. for $\eta = 0$, and the axial stress at the crack tip in the crack plane is given by:

$$\sigma_{yy} \Big|_{x=a, y=0} = \sigma_{\eta\eta} \Big|_{\xi=\xi_0, \eta=0} = S \left(1 + 2 \frac{a}{b} \right). \quad (32)$$

Note that it becomes extremely large in the case of a very slender crack (i.e. $b \approx 0$).

It is also worth examining the predicted stress distribution along the crack extended line i.e. ($y = 0$) in the crack plane. Since on the positive x -axis, $\eta = 0$, and the shear stress $\sigma_{\xi\eta}$ is proportional to $\sin(2\eta)$ (see Eq.(30)), it follows that: $\sigma_{\xi\eta} = \sigma_{xy} = 0$, and $\sigma_{\eta\eta} = \sigma_{yy}$, $\sigma_{\xi\xi} = \sigma_{xx}$ (see also the definition of the elliptical coordinates given by Eq. (22)). As mentioned, for a location far from the crack tip ($x = a, y = 0$), the axial stress σ_{yy} is equal to the applied load S while the lateral stress σ_{xx} becomes null, as it should be.

It is also worth comparing the elastic stress distribution given by Eq.(28)-(30) with the Westergaard elastic stress field (see Eq.(19)). As an example, in Fig. 24-25 are shown the evolution of the normalized axial stress σ_{yy}/S , and lateral stress σ_{xx}/S in the plane of the crack (i.e. $y = 0$) as a function of the distance from the crack tip (which corresponds to $x = a$) for an elliptical crack characterized by $a = 4$ mm and $b = 0.5$ mm. The variation of the stresses corresponding to a distance from the crack tip less than 25% of the crack semi-length, a , are also shown. While according to either solution the axial stresses σ_{yy} have a similar variation and are

very close, the lateral stresses σ_{xx} are completely different, since according to the exact solution σ_{xx} is no longer equal to σ_{yy} (see Eq.(28)-(29)). As expected the most difference between the two analytical solutions is in the region very near the crack tip ($x = a$) (see the zooms in Fig. 14-15). As it is well known, at the crack tip the classical solution predicts an infinite value for both σ_{xx} and σ_{yy} while according to the solution derived by Revil-Baudard and Cazacu (2018) the axial stress, σ_{yy} , has an extremely large but finite value (see Eq. (32)) while $\sigma_{xx} = 0$ because it satisfies the boundary conditions (the crack surface is traction free).

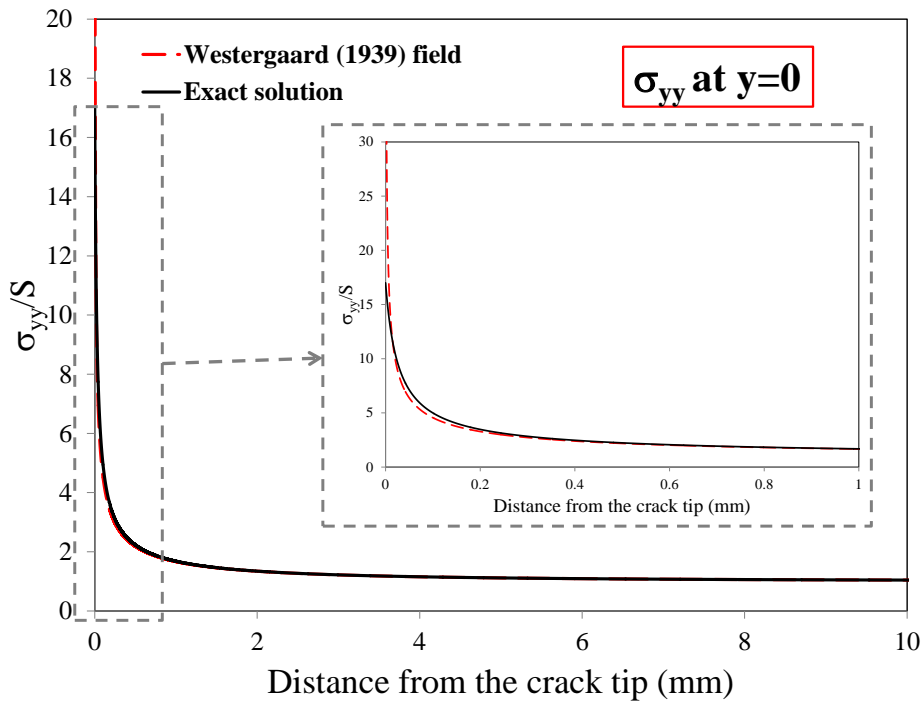


Figure 14. Evolution of the elastic axial stress σ_{yy}/S in the plane of the crack ($y = 0$) for an elliptical crack characterized by $a = 4\text{mm}$ and $b = 0.5\text{mm}$. Comparison between the exact solution given by Eq. (28)-(30) and the solution of Westergaard (1939), respectively. The zoom shows the near-tip stress distribution.

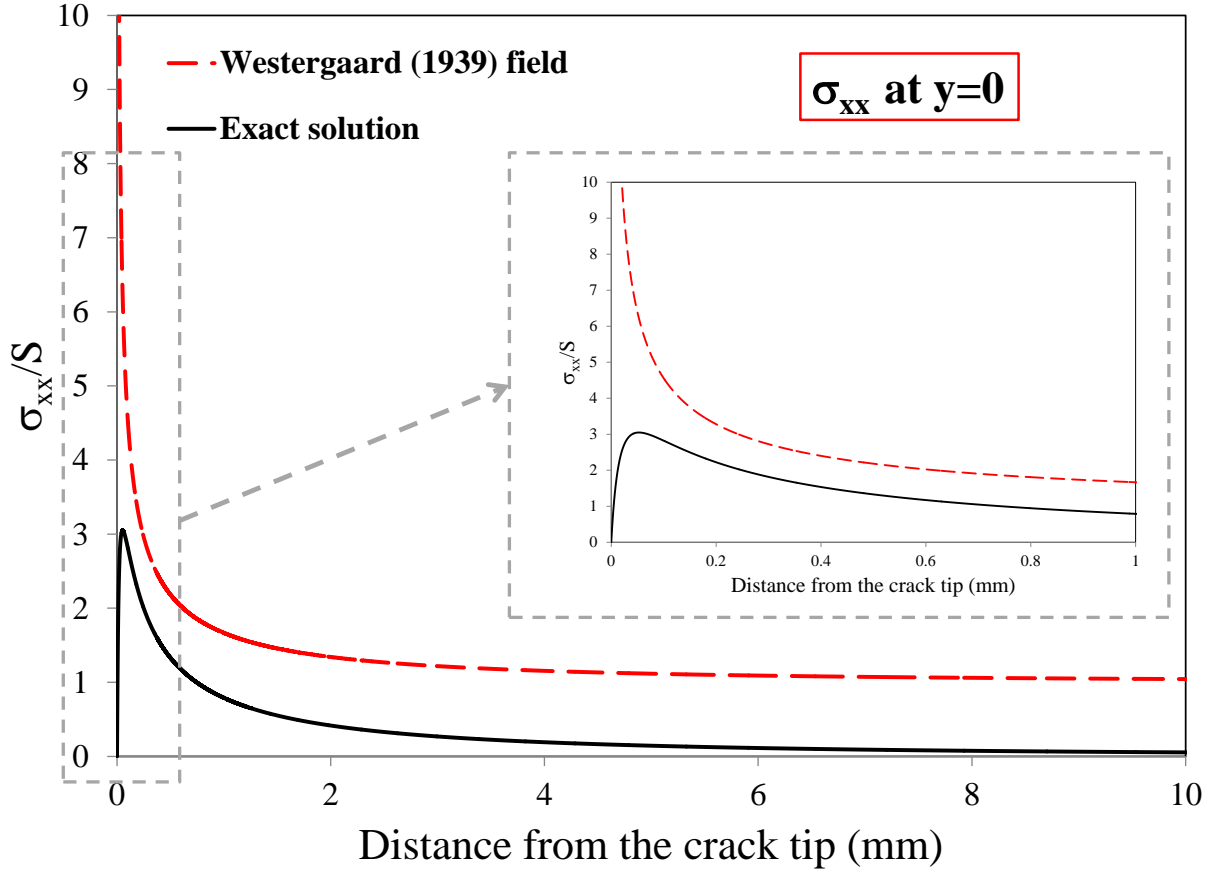


Figure 15: Evolution of the elastic lateral stress σ_{xx}/S in the plane of the crack ($y=0$) for an elliptical crack characterized by $a=4\text{mm}$ and $b=0.5\text{mm}$. Comparison between the exact solution given by Eq. (28)-(30) and the solution of Westergaard (1939), respectively. The zoom shows the near-tip stress distribution.

It is also worth examining the predicted elastic stress distribution in the plane normal to the crack i.e. ($x = 0$) according to the exact elastic solution given by Eq. (28)-(30) and the classical elastic solution of Westergaard (1939). For the same crack geometry, the results are shown in Fig. 16-17. While the two solutions for the axial stress $\sigma_{yy}|_{x=0}$ are very close, and show the same type of evolution with the distance from the crack tip (which in this plane corresponds to $x = 0, y=b$) the lateral stresses $\sigma_{xx}|_{x=0}$ are completely different, the Westergaard (1939) solution largely overpredicting the exact values. Indeed, for $x = 0$, we have $\cos(\eta)=0$ (see Eq. (22)), so:

$\sigma_{\eta\eta} = \sigma_{xx}$, $\sigma_{\xi\xi} = \sigma_{yy}$, and $\sigma_{xy} = 0$. Thus, according to the exact solution (see Eq.(28)-(29)) at the crack tip $\sigma_{xx} = -S$, and $\sigma_{yy} = 0$, whereas according to Westergaard's solution $\sigma_{xx} = 0$.

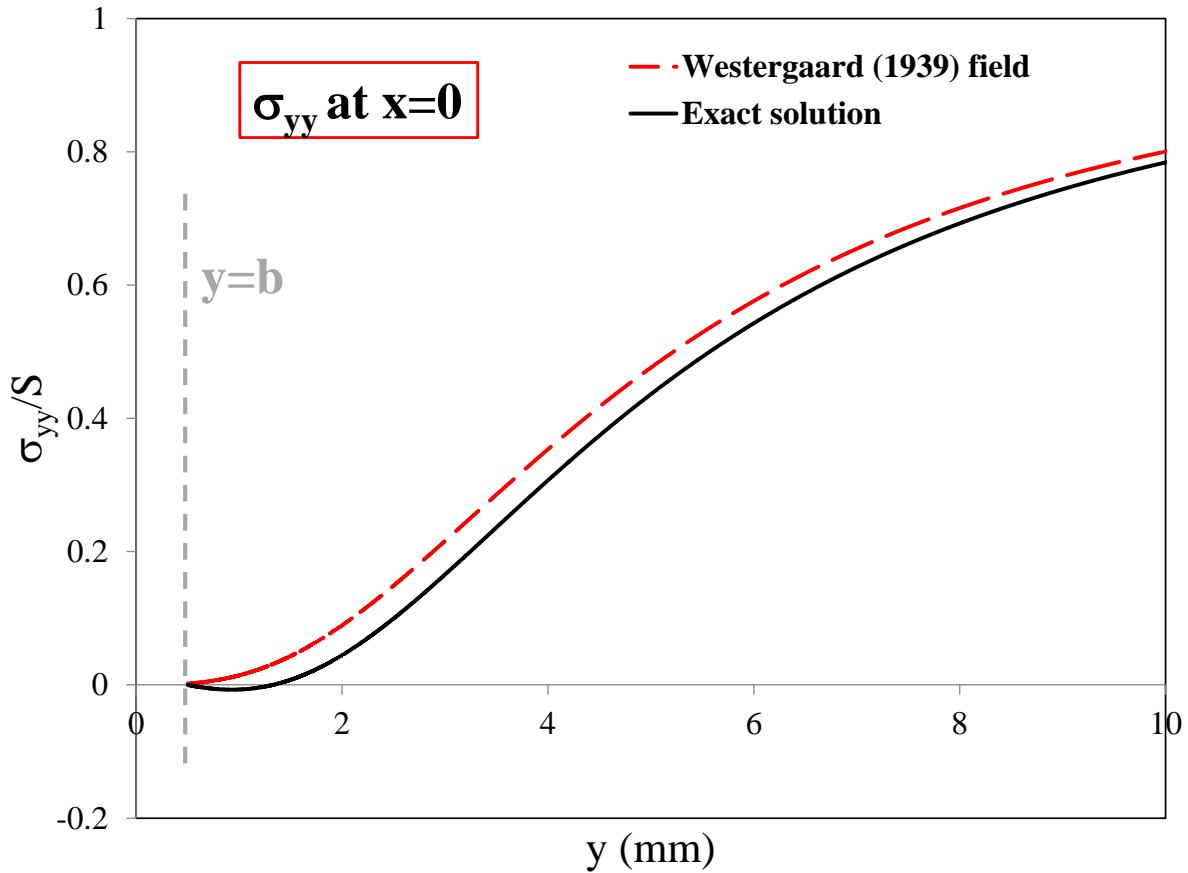


Figure 16: Evolution of the elastic axial stress σ_{yy}/S in the plane normal to the crack ($x = 0$) for an elliptical crack characterized by $a = 4$ mm and $b = 0.5$ mm. Comparison between the exact solution given by Eq. (28)-(29) and the solution of Westergaard (1939), respectively.

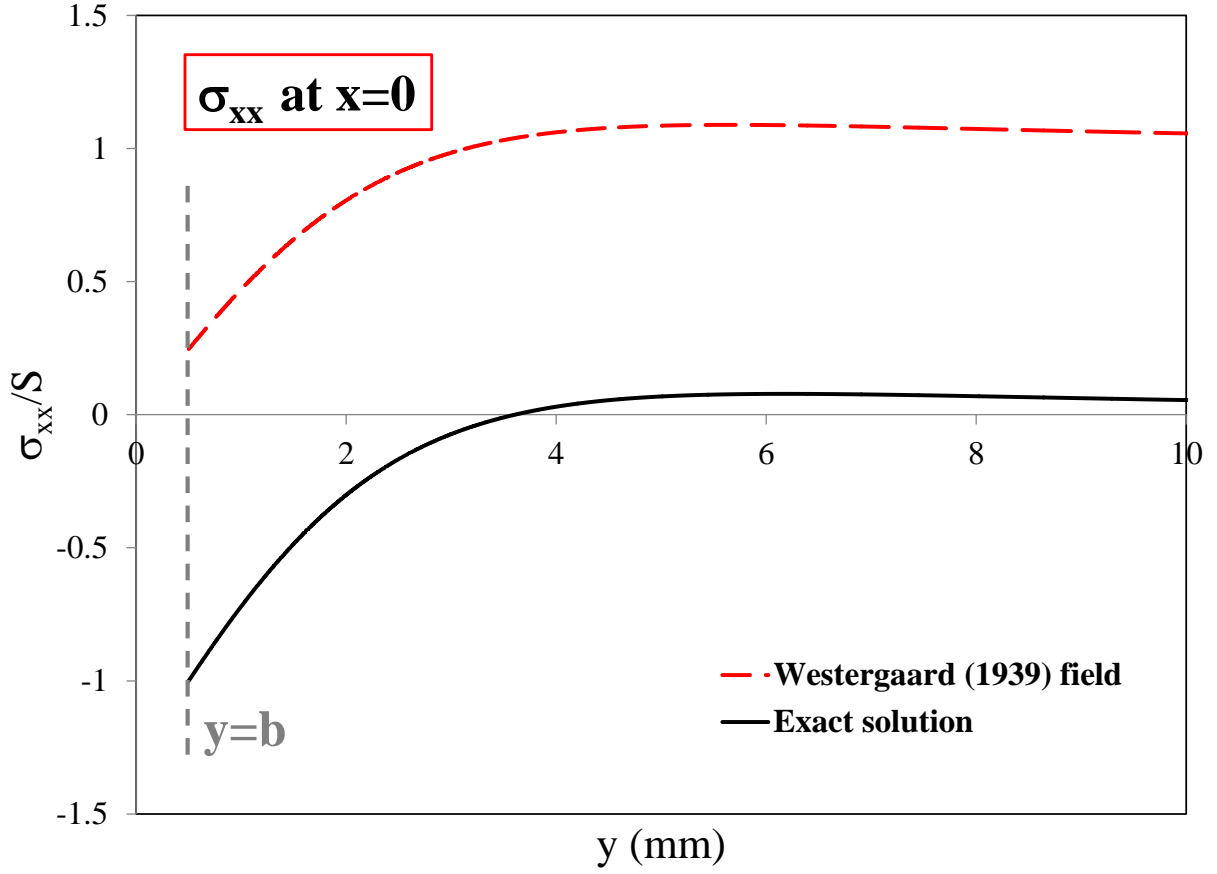


Figure 17: Evolution of the elastic axial stress σ_{xx}/S in the plane normal to the crack ($x = 0$) for an elliptical crack characterized by $a = 4$ mm and $b = 0.5$ mm. Comparison between the exact solution given by Eq.(28)-(30), and the solution of Westergaard (1939), respectively.

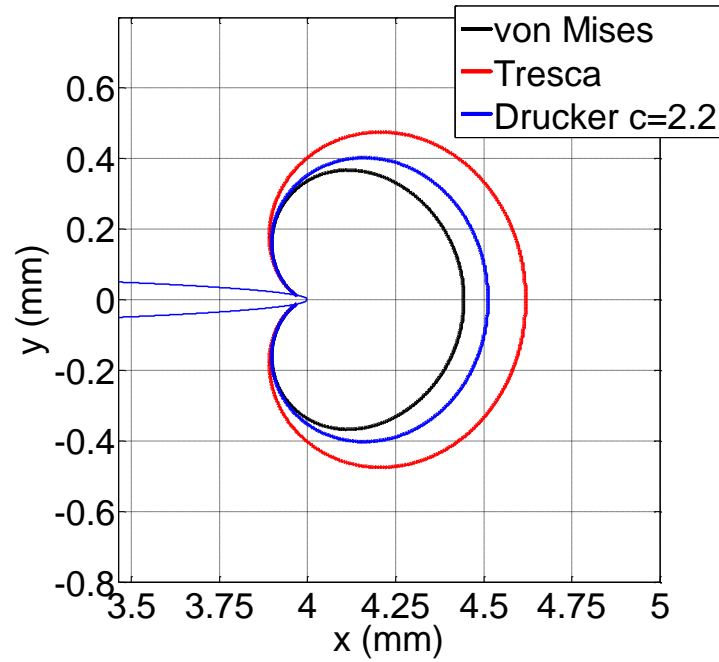
3.2. Plastic zone in front of a crack

For a sufficiently large applied load S , the material enters the plastic regime. The onset of yielding, according to any isotropic yield criterion can be easily calculated using the elastic stress distribution. Let d denote the extent of the plastic zone measured from the crack tip in the crack plane. If d is calculated using the classical near-tip elastic stress field given by Eq.(21), all the isotropic yield criteria predict:

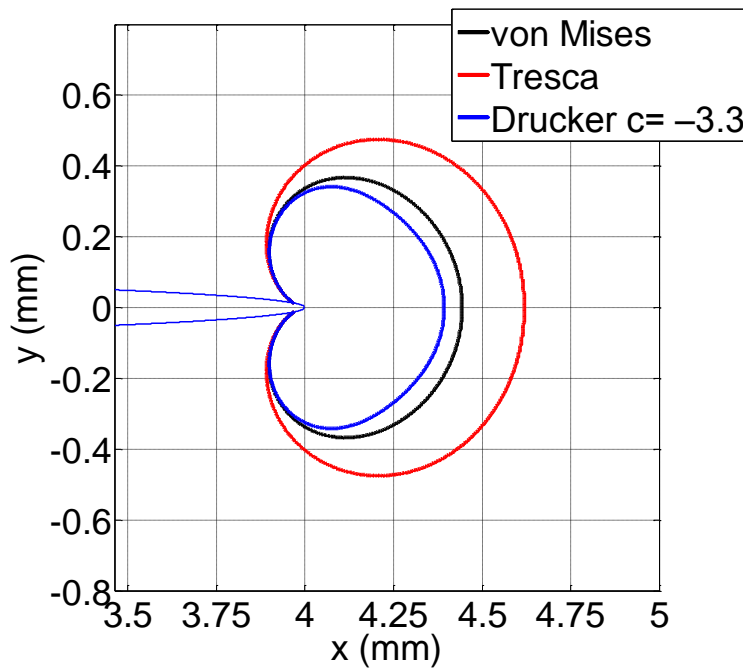
$$d = \frac{1}{2\pi} \left(\frac{K_I}{\sigma_T} \right)^2 \quad \text{with} \quad K_I = S\sqrt{\pi a} \quad , \quad (33)$$

(see for example, Sun and Jin (2012)). As already mentioned, the exact elastic stress field given by Eq. (28)-(30) is not axisymmetric. Therefore, the onset of yielding and the extent of the plastic zone in the vicinity of the crack depend on the yielding characteristics of the given isotropic material. As an example, in Fig.18 are shown the plastic zones in front of the crack corresponding to an external loading $S = \sigma_T/2$ that were obtained using Eq. (28)-(30) in conjunction with Tresca, von Mises, and Drucker (1949) yield criterion corresponding to $c = 2.2$ and $c = -3.3$, respectively. Let us denote as d_{Tresca} , d_{Mises} , and $d_{Drucker}$ the extent of the plastic zone corresponding to the respective yield criteria. It is worth noting that if yielding is described by Tresca's criterion the extent of the plastic zone is the largest. Also, note the strong sensitivity of $d_{Drucker}$ to the value of the parameter c , which is related to the ratio between the yield stresses in uniaxial tension and pure shear. Specifically, for $c = 2.2$ the plastic zone is larger than for $c = 0$ (which corresponds to von Mises), which in turn is larger than the plastic zone for a material characterized by $c = -3.3$. Moreover, the difference between the extent of the plastic zone size of a material with yielding described by Tresca and von Mises is significant, for example for $S = \sigma_T/2$: $(d_{Tresca} - d_{Mises}) / d_{Mises} = 39\%$.

These conclusions hold true irrespective of the applied loading (see Revil-Baudard and Cazacu (2018)). Specifically, irrespective of the applied load S , for materials with yielding described by Drucker (1949) criterion: $d_{Drucker} < d_{Tresca}$; for materials with yielding behavior corresponding to $c > 0$ the plastic zone size is larger than for a Von Mises material ($c = 0$) while the reverse holds true for materials with $c < 0$. As discussed in Revil-Baudard et al., 2018 for a material with $c > 0$: $\sigma_T / \tau_Y \in (\sqrt{3}, 2)$, and its yield surface is interior to the von Mises yield surface; for a material with $c < 0$: $\sigma_T / \tau_Y < \sqrt{3}$, and the corresponding yield surface is exterior to that according to von Mises yield criterion. Thus, these results lead to more general conclusions. Namely, if the yielding behavior is best described with a criterion represented by an even yield function, the extent of the plastic zone is always smaller than d_{Tresca} . As pointed out in Revil-Baudard and Cazacu (2018), the greater is the ratio σ_T / τ_Y of a material, the larger the size of the plastic zone is.



(a)



(b)

Figure 18: Predicted extent of the plastic zone at the crack tip ($a=4\text{mm}$, $b=0.1\text{mm}$) for uniaxial loading at $S/\sigma_T = 0.5$. Influence of the ratio between the yield stresses in uniaxial tension and pure shear on the size of the plastic zone. (a) Comparison between a von Mises material, a Tresca material and a Drucker (1949) material characterized by $c=2.2$, i.e. $\sqrt{3} < \sigma_T/\tau_Y < 2$); (b) Comparison between a von Mises material, a Tresca material and a Drucker (1949) material characterized by $c= -3.3$, i.e. $\sigma_T/\tau_Y < \sqrt{3}$).

3.2.1. Analytical expression for the size of the plastic zone for material with yielding described by Tresca yield criterion

We also showed that if yielding is described by Tresca's or von Mises yield criterion, it is possible to obtain explicit relations for the extent of the plastic zone in the crack plane. The proof is summarized in the following. The exact solution for the elastic stresses in the plane of the crack ($y=0$) is given by Eq. (28)-(30) with $\eta=0$. Therefore, $\sigma_{\eta\xi}=0$, and the principal stresses are: $\sigma_{\eta\eta} > \sigma_{\xi\xi} \geq 0$. Consequently, Tresca yield criterion writes:

$$\sigma_{\eta\eta} = \sigma_T. \quad (34)$$

Finding the extent of the plastic zone, measured from the crack tip, i.e. $d_{Tresca} = c \cosh \xi - a$, reduces to solving an algebraic equation for $w = \tanh \xi$ which is given by:

$$\alpha w^3 + (\gamma - \beta) w^2 - \gamma = 0, \quad (35)$$

The coefficients γ and β involved in Eq.(35) depend only on the crack dimensions, namely,

$$\gamma = \sinh^2 \xi_0 (1 + e^{-2\xi_0}), \quad (36)$$

$$\beta = 1 + e^{-2\xi_0} - \sinh \xi_0, \quad (37)$$

while the coefficient α depends on the applied loading σ_T / S and the crack geometry ($\tanh(\xi_0) = b / a$), and is given by:

$$\alpha = 1 - \cosh 2\xi_0 + 2(\sigma_T / S). \quad (38)$$

Since b is much smaller than a , the only non-trivial positive solution of Eq. (35) is:

$$w = (\beta - \gamma) / \alpha \quad (39)$$

Further, using Eq. (22), we obtain that:

$$d_{Tresca} = \frac{a}{\cosh(\xi_0)} \left(\cosh \left(\tanh^{-1} \left(\frac{\beta - \gamma}{1 - \cosh 2\xi_0 + 2(\sigma_T / S)} \right) \right) - \cosh(\xi_0) \right). \quad (40)$$

Note that the extent of the plastic zone depends of the applied loading σ_T / S and the crack geometry through ξ_0 .

3.2.2. Analytic expression for the size of the plastic zone for a material with yielding described by von Mises yield criterion

As mentioned, the exact elastic solution in the crack plane is such that $\sigma_{\eta\xi}=0$. Therefore, finding the extent of the plastic zone measured from the crack tip in the crack plane for a material with yielding described by von Mises yield criterion, reduces to solving a sixth-order algebraic equation for $w = \tanh \xi$ obtained by substituting $\sigma_{\eta\eta}$ and $\sigma_{\xi\xi}$ given by Eq. (28)-(29) with $\eta = 0$ into the expression of the von Mises yield condition for 2-D loadings, i.e.,

$$\left(\sigma_{\eta\eta} + \sigma_{\xi\xi}\right)^2 + 3\left(\sigma_{\eta\eta} - \sigma_{\xi\xi}\right)^2 = 4\sigma_T^2 ,$$

Since b is much smaller than a , this sixth-order equation for w has a unique positive solution. Further using the relation between the Cartesian and elliptical coordinates (see Eq.(22)), we obtain that:

$$d_{Mises} = \frac{a}{\cosh(\xi_0)} \left(\cosh \left(\tanh^{-1} \left[\frac{3}{2A_1} \left(B_1 - \sqrt{B_1^2 - 4A_1C_1/3} \right) \right] \right) - \cosh(\xi_0) \right) . \quad (41)$$

In the above relation,

$$A_1 = 1 + \cosh^2(2\xi_0) - 4e^{-4\xi_0} (\sigma_T / S), \quad (42)$$

depends on the crack geometry through ξ_0 , on the applied loading S , and on σ_T , while B_1 and C_1 depend only on the crack geometry:

$$B_1 = \frac{2}{3} \left[1 + e^{-2\xi_0} + 3 \cosh(2\xi_0) (\gamma + \sinh(2\xi_0)) \right] \quad (43)$$

$$C_1 = \frac{1}{3} \left[\left(1 + e^{-2\xi_0} \right)^2 + 3 (\gamma + \sinh(2\xi_0))^2 \right] \quad (44)$$

with γ given by Eq. (36).

In summary, using the explicit formulas given by Eq. (40) and Eq.(41), it is possible to obtain an estimate of the plastic zone of any given isotropic material that displays the same yielding response in tension and compression. Specifically, the extent of its plastic zone, d , is always less than d_{Tresca} ; if the material is characterized by $\sigma_T / \tau_Y < \sqrt{3}$, then $d > d_{Mises}$ while the reverse holds true if $\sigma_T / \tau_Y > \sqrt{3}$.

4. Cazacu (2018) plastic potential for orthotropic materials Cazacu (2018)

The influence of plastic anisotropy of materials on fatigue life remains a major concern. Key in advancing the understanding is an appropriate representation of the material symmetries induced by the fabrication process (e.g. transverse isotropy induced by extrusion; orthotropy induced by rolling). A new anisotropic plastic potential was developed in the framework of the theory of representation of tensor functions (Cazacu, 2018). This potential and its predictive capabilities are summarized in the following.

Cazacu (2018) orthotropic criterion is expressed as:

$$F(J_2^0, J_3^0) = (J_2^0)^4 - \alpha (J_2^0)(J_3^0)^2 \quad (45)$$

In Eq.(45), α is a parameter, and J_2^0, J_3^0 are the orthotropic invariants of the stress deviator, $\boldsymbol{\sigma}'$, their expressions relative to the coordinate system associated with the $(\mathbf{x}, \mathbf{y}, \mathbf{z})$ orthotropy axes of the material being given by:

$$J_2^0 = \frac{a_1}{6} (\sigma'_{xx} - \sigma'_{yy})^2 + \frac{a_2}{6} (\sigma'_{yy} - \sigma'_{zz})^2 + \frac{a_3}{6} (\sigma'_{xx} - \sigma'_{zz})^2 + a_4 \sigma'^2_{xy} + a_5 \sigma'^2_{xz} + a_6 \sigma'^2_{yz}, \quad (46)$$

and

$$\begin{aligned}
J_3^o &= \frac{1}{27}(b_1 + b_2)\sigma_{xx}'^3 + \frac{1}{27}(b_3 + b_4)\sigma_{yy}'^3 + \frac{1}{27}[2(b_1 + b_4) - b_2 - b_3]\sigma_{zz}'^3 \\
&\quad - \frac{1}{9}(b_1\sigma_{yy}' + b_2\sigma_{zz}')\sigma_{xx}'^2 - \frac{1}{9}(b_3\sigma_{zz}' + b_4\sigma_{xx}')\sigma_{yy}'^2 \\
&\quad - \frac{1}{9}[(b_1 - b_2 + b_4)\sigma_{xx}' + (b_1 - b_3 + b_4)\sigma_{yy}']\sigma_{zz}'^2 \\
&\quad + \frac{2}{9}(b_1 + b_4)\sigma_{xx}'\sigma_{yy}'\sigma_{zz}' - \frac{\sigma_{xz}'^2}{3}[2b_9\sigma_{yy}' - b_8\sigma_{zz}' - (2b_9 - b_8)\sigma_{xx}'] \\
&\quad - \frac{\sigma_{xy}'^2}{3}[2b_{10}\sigma_{zz}' - b_5\sigma_{yy}' - (2b_{10} - b_5)\sigma_{xx}'] - \frac{\sigma_{yz}'^2}{3}[2b_7\sigma_{xx}' - b_6\sigma_{yy}' - (2b_7 - b_6)\sigma_{zz}'] \\
&\quad + 2b_{11}\sigma_{xy}'\sigma_{xz}'\sigma_{yz}'
\end{aligned} \tag{47}$$

with a_i ($i=1\dots6$) and b_k ($k=1\dots11$) being constants. Note that J_2^o is a homogenous polynomial of degree two in its arguments, insensitive to hydrostatic pressure, which satisfies the symmetry restrictions associated with orthotropy. When all the coefficients $a_i=1$, J_2^o reduces to the classic isotropic invariant J_2 . On the other hand, J_3^o is a homogenous third-order polynomial in stresses that reduces to the isotropic invariant J_3 if all $b_k=1$, it is insensitive to hydrostatic pressure, and satisfies the orthotropic symmetries. For more details concerning the derivation of these orthotropic invariants, see the monograph of Cazacu et al. (2019). The effective stress, $\bar{\sigma}$ associated to the Cazacu (2018) criterion is given by:

$$\bar{\sigma} = m \left[(J_2^o)^4 - \alpha (J_2^o)(J_3^o)^2 \right]^{1/8}, \tag{48}$$

with m being a constant defined such that for uniaxial tension in the \mathbf{x} - direction the effective stress reduces to the yield stress, i.e.

$$m = \frac{3\sqrt{2}}{\left\{ \left[27(a_1 + a_3)^3 - 8\alpha(b_1 + b_2)^2 \right] (3a_1 + 3a_3) \right\}^{1/8}} \tag{49}$$

For general 3-D stress conditions Cazacu (2018) orthotropic criterion involves 17 anisotropy coefficients (for proof of this statement see Cazacu (2018)).

In the plane of the sheet (RD, TD), this orthotropic criterion predicts the following dependence of the normalized uniaxial flow stress $\sigma(\theta)/\sigma(0)$ on the angle θ .

$$m(\sigma(\theta)/\sigma(0)) = \left\{ \left[(a_1/6 + a_3/6)\cos^4\theta + (a_4 - a_1/3)\cos^2\theta\sin^2\theta + (a_1/6 + a_2/6)\sin^4\theta \right]^4 - \alpha \left[\begin{array}{l} \cos^6\theta(b_1 + b_2)/27 + \sin^6\theta(b_3 + b_4)/27 \\ -\sin^2\theta\cos^4\theta(b_1 + 3b_3 - 6b_{10})/9 \\ -\sin^4\theta\cos^2\theta(b_4 - 3b_5)/9 \end{array} \right]^2 \times \left[\begin{array}{l} (a_1/6 + a_3/6)\cos^4\theta \\ + (a_4 - a_1/3)\cos^2\theta\sin^2\theta \\ + (a_1/6 + a_2/6)\sin^4\theta \end{array} \right] \right\}^{-1/8} \quad (50)$$

Assuming associated flow rule, the Lankford coefficients $r(\theta)$ are calculated using equation:

$$r(\theta) = \frac{d\varepsilon'_{yy}}{d\varepsilon'_{zz}} = - \frac{\sin^2\theta d\varepsilon_{xx} - \sin(2\theta)d\varepsilon_{xy} + \cos^2\theta d\varepsilon_{yy}}{d\varepsilon_{xx} + d\varepsilon_{yy}}$$

with the components of the plastic strain increment as $d\varepsilon$ being calculated assuming associated flow rule, i.e.

$$d\varepsilon = d\lambda \frac{\partial \bar{\sigma}}{\partial \sigma}, \quad (51)$$

where $d\lambda \geq 0$ denotes the plastic multiplier. The specific expressions for $\frac{\partial \bar{\sigma}}{\partial \sigma_{ij}}$ $i, j = 1 \dots 3$ given

by

$$\frac{\partial \bar{\sigma}}{\partial \sigma_{ij}} = \left(\frac{m}{8} \right) \left\{ \left[4(J_2^0)^3 - \alpha(J_3^0)^2 \right] \frac{\partial J_2^0}{\partial \sigma_{ij}} - 2\alpha(J_3^0)(J_2^0) \frac{\partial J_3^0}{\partial \sigma_{ij}} \right\} \times \left[(J_2^0)^4 - \alpha(J_2^0)(J_3^0)^2 \right]^{-7/8} \quad (52)$$

It is also worth noting that if in the Cazacu (2018) orthotropic criterion the coefficient α is set equal to zero, Hill's orthotropic criterion is recovered. Let us recall that in the coordinate system Oxyz associated with the axes of orthotropy of the material Hill (1948) yield criterion is expressed as:

$$F(\sigma_{yy} - \sigma_{zz})^2 + G(\sigma_{zz} - \sigma_{xx})^2 + H(\sigma_{xx} - \sigma_{yy})^2 + 2L\sigma_{yz}^2 + 2M\sigma_{zx}^2 + 2N\sigma_{xy}^2 = \bar{\sigma}^2 \quad (53)$$

where F, G, H, L, M, N are anisotropy coefficients of the material.

Note also that according to Cazacu (2018) model yielding under equibiaxial tension in the plane (\mathbf{x}, \mathbf{y}) occurs when $\sigma_{xx} = \sigma_{yy} = \sigma_b^T$ with

$$\frac{\sigma_b^T}{\sigma_0} = \frac{1}{B} \left[\left(\frac{a_2 + a_3}{6} \right)^4 - \alpha \left(\frac{2b_1 - b_2 - b_3 + 2b_4}{27} \right)^2 (a_2 + a_3) / 6 \right]^{-1/8} \quad (54)$$

Yielding under pure shear in the (x,y) plane (or (RD, TD) for a rolled sheet, with RD denoting the rolling direction, and TD the transverse direction) is equal to:

$$\tau_{RD-TD} = \frac{\sigma_0}{B\sqrt{a_4}}. \quad (55)$$

In summary, for description of plastic properties in the plane (\mathbf{x}, \mathbf{y}) or (RD-TD) the criterion involves ten anisotropy coefficients $a_1, a_2, a_3, a_4, b_1, b_2, b_3, b_4, b_5, b_{10}$ and the parameter α . These parameters can be determined by minimizing an error function of the form:

$$E(a_1, a_2, a_3, a_4, b_1, b_2, b_3, b_4, b_5, b_{10}, \alpha) = \sum_i^n \eta_i \left(1 - \frac{(\sigma_\theta)_i^{th}}{(\sigma_\theta)_i^{data}} \right)^2 + \sum_j^m \gamma_j \left(1 - \frac{(r_\theta)_j^{th}}{(r_\theta)_j^{data}} \right)^2 + \delta \left(1 - \frac{(\sigma_b^T)_i^{th}}{(\sigma_b^T)_i^{data}} \right)^2 \quad (56)$$

In the above equation, “n” and “m” represent the number of experimental yield stresses and r-values, respectively corresponding to different orientations θ that are available, the superscript indicates whether the respective value is experimental or it is calculated using the above expressions for theoretical r-values and yield stresses while η_i , γ_j and δ are weight factors. As an example, in Figure (a)-(b) are shown the predicted variation of the yield stresses and r-values in the plane of the plate or sheet (i.e. (\mathbf{x}, \mathbf{y}) or (RD, TD)) according to the Cazacu (2018) and Hill (1948) criterion, respectively, in comparison with the measured yield stresses for an Al 6022-T4 Al sheet (data after Barlat et al. (1997)). The stresses are normalized by the uniaxial tensile yield stress in the rolling direction. The numerical values of the coefficients involved in

the criterion that were determined from the experimental yield stresses and r-values for $\theta = 0^\circ$, 30° , 45° , 60° , 90° and the tensile equibiaxial yield stress σ_b^T are: $a_1 = 0.709$, $a_2 = 1.36$; $a_3 = 1.18$, $a_4 = 0.96$, $b_1 = 0.2$, $b_2 = -1.334$, $b_3 = -1.53$, $b_4 = 0.94$, $b_5 = 1.18$, $b_{10} = 0.988$, and $\alpha = 1.5$. The numerical values of the Hill (1948) coefficients for this material, calculated based on the experimental r-values at $\theta = 0^\circ$, 45° , 90° are: $F=0.706$, $G=0.587$, $H=0.413$, and $N=1.27$. Note that only the Cazacu (2018) criterion describes with accuracy both the anisotropy in yielding and r-values for this Al sheet (see Fig. 19). The projection in the $(\sigma_{xx}, \sigma_{yy})$ plane of the yield surface corresponding to $\sigma_{xy} = 0$, according to Cazacu (2018) criterion and Hill (1948) criterion, respectively are shown in Fig. 20. Note that in contrast to the Hill (1948) criterion, the Cazacu (2018) criterion captures with accuracy both the anisotropy in yield stresses and r-values. Moreover, Hill (1948) criterion underpredicts the experimental equibiaxial yield stress.

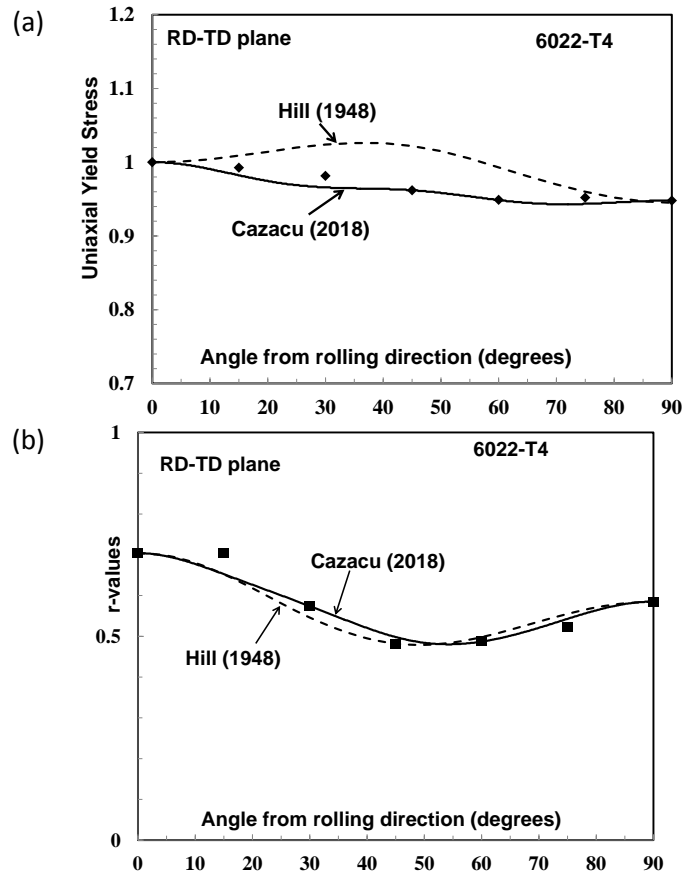


Figure 19. Predicted anisotropy according to the Cazacu (2018) orthotropic criterion (interrupted line) and Hill (1948) criterion for an Al alloy AA 6022-T4. (a) Uniaxial yield stress variation; (b) Lankford coefficients. Data

(symbols) from Barlat et al. (1997). Stresses are normalized by the uniaxial yield stress in tension in the rolling direction.

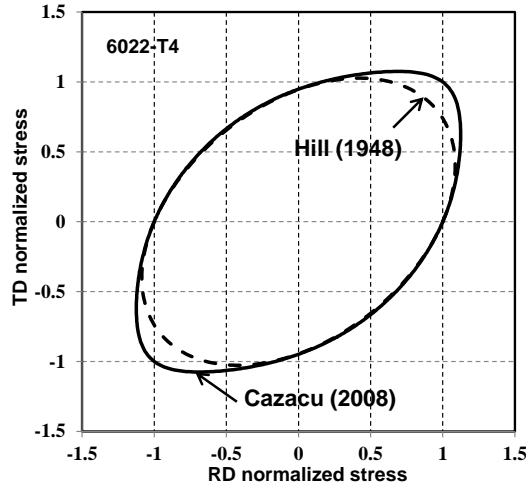


Figure 20. Projection of the yield surface in the plane (σ_x, σ_y) (with $\sigma_{xy} = 0$) for AA 6022-T4 as predicted by the orthotropic Cazacu (2018) yield criterion and Hill (1948) criterion.

5. Conclusions

Fatigue failure is a continuous concern for a large variety of military and civilian applications. The current approach to fatigue is based on empirical data. Prediction of failure due to fatigue will substantially reduce operational burdens due to logistics services while enabling equipment readiness. As part of this research project, new findings that enable physical understanding of the phenomenon were obtained.

- It was demonstrated that in an isotropic material the extent of the plastic zone that develops near a crack depends significantly on the ratio σ_T / τ_Y between the yield stresses in uniaxial tension and in pure shear.
- This finding was established based on a new solution for the elastic stresses in the vicinity of a central crack in a plate subject to uniaxial tension. In contrast to the classical solution based on Westergaard potential, this new solution satisfies the boundary conditions (shear stress and normal stress are zero along the crack surface) and as such it is not axisymmetric along the crack line.
- Using this new elastic stress field solution, the effect of the particularities of yielding on the plastic zone was put into evidence.

- It was demonstrated that irrespective of the applied far-field loading, if yielding is described by Tresca criterion the plastic zone that develops near a crack is larger than in the case when yielding is governed by the von Mises criterion. For example, for an applied load $S=0.75 \sigma_T$ the extent of *plastic zone for a Tresca material is 58% larger than* that for a material with yielding described by the *von Mises* yield criterion.
- In general, irrespective of the external loading *the larger is the ratio between the yield stresses in uniaxial tension and pure shear of a material the larger is the extent of the plastic zone*. The upper bound for the size of the plastic zone is obtained for a Tresca type material ($\sigma_T / \tau_Y = 2$).
- A new isotropic strain-rate potential for isotropic pressure-insensitive metallic materials with the same response in tension and compression was also developed. The new potential depends on both invariants of the strain-rate deviator. The relative weight of the two invariants is described by a material parameter β . Depending on the sign of the parameter β , the new plastic potential is either interior to the von Mises strain-rate potential ($\beta < 0$), coincides with it ($\beta = 0$) or it is exterior to it. The range of variation of this parameter such as to ensure convexity of the potential was analytically determined.
- In general, for tensile loadings *the larger is the ratio between the yield stresses in uniaxial tension and pure shear of a material the slowest is the rate of damage growth*. The fastest rate of damage growth is obtained for a Tresca type material. For compressive loading, the reverse holds true. Namely, the fastest rate of void collapse correspond to Tresca type material.
- A new plastic potential accounting for orthotropy was developed. Its improved predictive capabilities with respect to classic formulations were demonstrated.

The research presented opens new avenues for advancing our understanding of the influence of the plastic deformation on every aspect of the fatigue crack propagation. Moreover, the models developed are to assist in the development of enhanced new materials for which the rate of crack propagation is substantially decreased.

6. Resulting Publications during Reporting Period

Monograph:

O. Cazacu, B. Revil-Baudard, N. Chandola [2019] *Plasticity-Damage Couplings: From Single Crystal to Polycrystalline Materials*, Springer, 2019; 518 pp., <https://doi.org/10.1017/978-3-319-92922-4>, ISBN 978-3-319-92921-7 (<https://www.springer.com/gb/book/9783319929217>)

Book Chapter:

J.L. Alves and O. Cazacu [2017] Effect of the third-invariant of the stress deviator on the response of porous solids with pressure-insensitive matrix, Chapter 5 in: *From microstructure investigations to multiscale modeling : bridging the gap*”, Wiley-ISTE, 2017, Eds: S. Bouvier, D.Brancherie, P. Feisel, A. Ibrahimovic Wiley-ISTE, 2017, ISBN:978-1-78630-259-5.

Refereed Journal Publications

1. O. Cazacu and B. Revil-Baudard [2016] New analytic criterion for porous solids with pressure-insensitive matrix, *Int. J. Plasticity*, 89, 66-84.
2. O. Cazacu [2018]. New yield criteria for isotropic and textured metallic materials. *International Journal of Solids and Structures*, 139, 200-210.
3. B. Revil-Baudard, O. Cazacu, N. Chandola [2018] Effect of the ratio between the yield stresses in uniaxial tension and pure shear on the shape and size of the plastic zone near a crack, *Int. J. Plasticity*, 102, 101-117.
4. D. Savage, N. Chandola, O. Cazacu, Brandon A. McWilliams, Marko Knezevic [2018] Validation of recent analytical dilatational models for porous polycrystals using crystal plasticity finite element models with Schmid and non-Schmid activation laws (2018), *Mechanics of Materials* 126, 148-162.

References

1. Cazacu O, Revil-Baudard B (2017) New analytic criterion for porous solids with pressure insensitive matrix. *Int J Plast* 89:66–84
2. Cazacu O (2018) New yield criteria for isotropic and textured metallic materials. *Int J Solids Struct.* doi: <https://doi.org/10.1016/j.ijsolstr.2018.01.036>.
3. Cazacu, O., Revil-Baudard, B., Chandola, N., 2019. *Plasticity-Damage Couplings: From Single Crystal to Polycrystalline Materials.* Springer Nature <https://www.springer.com/gb/book/9783319929217> .
4. Revil-Baudard, B., Cazacu, O., Chandola, N., 2018. Effect of the yield stresses in uniaxial tension and pure shear on the size of the plastic zone near a crack. *Int J Plast* 102, 101–117.
5. Fekete, B., 2015. New energy-based low-cycle fatigue model for reactor steels. *Materials and Design*, 79, 42-52.
6. Coffin, L.F. 1974. Fatigue at high temperature – prediction and interpretation. *Proc.Inst. Mech. Eng.*, 188, 9/74.
7. Murakami, Y., Miller, K.J. 2005. What is fatigue damage? A view point from the observation of low cycle fatigue process. *Int. J. Fatigue*, 27, 769–779.
8. Surajit , S.K. Paul, Kumar, Sivaprasaa, S. , Dhar, S., Tarafder, S. 2010. Ratcheting and low cycle fatigue behavior of SA333 steel and their life prediction. *J. Nucl. Mater.*, 401, 17–24.
9. Zhang, Y., Hu, C.L., Zhao, Z., Li, A.P. , Xu, X.L., Shi, W.B. 2013. Low cycle fatigue behavior of a Cr–Mo–V matrix-type high-speed steel used for cold forging. *Mater. Des.*, 44, 612–621.

10. Li, Z., Han, J., Li, W., Pan, L. 2014. Low cycle fatigue behavior of Cr–Mo–V low alloy steel used for railway brake discs, *Mater. Des.*, 56, 146–157.
11. Lefebvre, D., Ellyin, F. 1984. Cyclic response and inelastic strain energy in low cycle fatigue. *Int. J. Fatigue*, 6, 55-67.
12. Chaboche, J-L., Kanoute, P., Azzouz, F., 2012. Cyclic inelastic constitutive equations and their impact on the fatigue life predictions. *Int. J. Plasticity*, 35, 44-66.
13. Taleb, L., Cailletaud, G., 2010. An updated version of the multimechanism model of cyclic plasticity. *Int. J. Plasticity*, 26, 859–874.
14. Rice JR, Tracey DM (1969) On the ductile enlargement of voids in triaxial stress fields. *J Mech. Phys Solids* 17:201–217
15. Cazacu O, Revil-Baudard B, Chandola N, Kondo D (2014c) New analytical criterion for porous solids with Tresca matrix under axisymmetric loadings. *Int J Solids Struct* 51:861–874
16. Stevenson, A., 1945. Complex potentials in two-dimensional elasticity. *Proceedings of the Royal Society of London. Series A. Mathematical and Physical Sciences* 184, 129–179.
17. Sun, C.T., Jin, Z.-H., 2012. *Fracture mechanics*. Academic Press, Boston. <https://doi.org/10.1016/B978-0-12-385001-0.00006-7>.
18. Westergaard, H.M., 1939. Bearing pressures and cracks. *Trans AIME, J. Appl. Mech.* 6, 49–53.
19. Drucker, D.C., 1949. Relation of Experiments to Mathematical Theories of Plasticity. *ASME Journal of Applied Mechanics* 16, 349–357.

20. Hill R., 1948. A theory of the yielding and plastic flow of anisotropic metals. In: Proceedings of the Royal Society of London A: Mathematical, Physical and Engineering Sciences. The Royal Society, pp 281–297

21. Barlat F, Becker RC, Hayashida Y, Maeda Y, Yanagawa M, Chung K, Brem JC, Lege DJ, Matsui K, Murtha SJ, Hattori, S.,1997. Yielding description for solution strengthened aluminum alloys. Int J Plast 13:385–401.